

# PIFLOW: PRINCIPLE-AWARE SCIENTIFIC DISCOVERY WITH MULTI-AGENT COLLABORATION

**Anonymous authors**

Paper under double-blind review

## ABSTRACT

Large Language Model (LLM)-based multi-agent systems (MAS) demonstrate remarkable potential for scientific discovery. Existing approaches, however, often automate scientific discovery using predefined workflows that lack rationality constraints. This often leads to aimless hypothesizing and a failure to consistently link hypotheses with evidence, thereby hindering the systematic reduction of uncertainty. Overcoming these limitations fundamentally requires a principled approach to exploration. We introduce `PiFlow`, an information-theoretical framework, treating automated scientific discovery as a structured uncertainty reduction problem guided by principles (e.g., scientific laws). In evaluations across three distinct scientific domains – discovering nanomaterial structures, bio-molecules, and superconductor candidates with targeted properties – our method significantly improves discovery efficiency, reflected by a 73.55% increase in the Area Under the Curve (AUC) of property values versus exploration steps, and enhances solution quality by 94.06% compared to a vanilla agent system. Overall, `PiFlow` serves as a Plug-and-Play method, establishing a novel paradigm shift in highly efficient automated scientific discovery, paving the way for more robust and accelerated AI-driven research.

## 1 INTRODUCTION

Large Language Model (LLM)-based Multi-Agent Systems (MAS) have significantly impacted automated scientific discovery (Minaee et al., 2024; Wang et al., 2023; Zhang et al., 2024c) across a wide range of fundamental fields, including chemistry (Liu et al., 2024; Ghafarollahi & Buehler, 2024a; Yang et al., 2024c; Inoue et al., 2024), biology (Xiao et al., 2024; Nagarajan et al., 2025; Averly et al., 2025; Ghafarollahi & Buehler, 2024b), physics (Jaiswal et al., 2024), and material science (Takahara et al., 2025; Ghafarollahi & Buehler, 2025; Ansari et al., 2024; Wan et al., 2024; Zhang et al., 2024b).

Although proficient in executing experiments within predefined workflows (Lu et al., 2024; Lai & Pu, 2025), these systems often generate hypotheses that lack clear direction, leading to the uncertainty establishing clear links between hypotheses and their supporting or refuting evidence (AI4Science & Quantum, 2023; Zhou et al., 2024; Baek et al., 2024; Schmidgall et al., 2025; Prabhakar et al., 2025; Xie et al., 2023a). Such a disconnect indicates inefficient exploration. Moreover, many of these approaches are tailored for specific tasks, often relying on meticulous prompt engineering that heavily incorporates domain knowledge (as detailed in Appendix D). Consequently, their ability to adapt to new scientific domains is often limited without substantial modifications (Zhang et al., 2025; Kumbhar et al., 2025). These issues culminate in three primary challenges: (a) **aimless hypothesizing**; (b) **unmaintained connections** between hypotheses and evidence during exploration, hindering systematic validation and (c) **limited generalization ability**, where systems effective in one scenario (e.g., material science) often require substantial rework to be applicable in others.

To address these limitations, we introduce `PiFlow`, an information-theoretic framework for structured uncertainty reduction in scientific discovery. Viewing scientific exploration as a game against an unknown and challenging nature, where robust strategies are paramount, `PiFlow` employs Min-Max optimization: **minimizing** cumulative regret for exploitation, while **maximizing** information gain for efficient hypothesis exploration. As a Plug-and-Play module, `PiFlow` integrates with MAS capable of hypothesizing and experimentation. Inspired by the challenge of navigating vast hypothesis spaces,

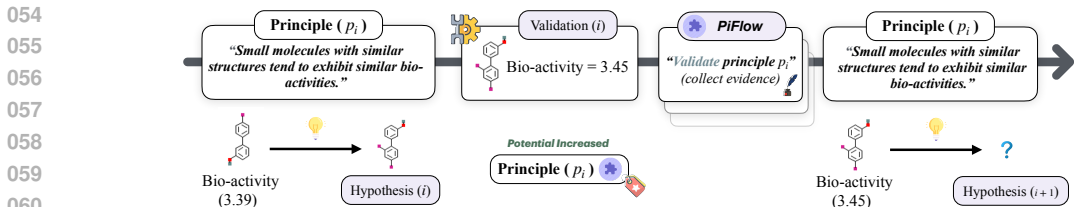


Figure 1: **Illustration of the potential of a scientific principle in drug discovery.** PiFlow directs exploration to prioritize hypotheses aligned with high-potential principles (or their variants), thereby iteratively guiding the discovery towards optimal candidate molecules.

PiFlow operates by using fundamental scientific principles, which may be initially proposed by or refined using LLMs.

The iterative selection of principles progressively reduces uncertainty in hypothesizing and the interpretation of evidence, dynamically steering exploration by prioritizing those scientific principles that offer the highest instructive value for continued exploration. Figure 1 illustrates PiFlow’s method for assessing and utilizing scientific principles within a drug discovery context.

This principle-aware approach yields systematic information gain: PiFlow selects high-potential principles and then guides hypothesizing via three actions, i.e., exploring, validating, or refining their scope and formulation. Thus, PiFlow progressively optimizes its guiding scientific principles to effectively steer hypothesizing. Furthermore, leveraging its Min-Max optimization, PiFlow theoretically achieves cumulative regret growth of  $\mathcal{O}(\sqrt{T})$  over  $T$  exploration steps (a detailed proof is provided in Appendix F). This sublinear regret underscores its guaranteed efficiency in navigating complex discovery landscapes. In summary, our contributions are:

- We propose a novel paradigm for **principle-aware scientific discovery**, built upon an information-theoretical foundation that offers convergence guarantees.
- We develop PiFlow, a **Plug-and-Play framework** that seamlessly integrates with existing MAS to enable focused exploration, thereby enhancing discovery efficiency and flexibility.
- We conduct **extensive experiments across three distinct scenarios**, demonstrating the broad applicability and significant performance improvements achieved by PiFlow.

## 2 RELATED WORK

### 2.1 LANGUAGE MODELS FOR SCIENTIFIC DISCOVERY

Recently, large language models (LLM) have advanced scientific discovery with automation and rational design (Ren et al., 2025; Ma et al., 2024). The internal knowledge of LLMs has demonstrated promising capability in focused chemical and material discovery (Yang et al., 2024c; Zhou et al., 2024; Pu et al., 2024; Ghafarollahi & Buehler, 2024c). While tool-integrated LLMs like SciAgents (Ghafarollahi & Buehler, 2024d), DARWIN (Xie et al., 2023a) and HoneyComb (Zhang et al., 2024a) improve domain-specific reasoning and recall of factual insights, they still struggle to integrate physicochemical laws effectively when refining insights for design, risking biased proposals and inefficient exploration due to inherent hallucinations of LLMs (Zhang et al., 2023b). Human-AI frameworks address this issue by leveraging the knowledge of domain experts (Reddy & Shojaee, 2024; Eythorsson & Clark, 2025), yet remain limited to the scope of hypothesis generation (Alkan et al., 2025), leading to insufficient exploration of complex chemical spaces (Luo et al., 2025). Surveys highlight persistent gaps in efficiency and interpretability (Zhang et al., 2024c; Han et al., 2024), underscoring the need for principled scientific discovery management beyond automated LLM reasoning (Ramos et al., 2024).

### 2.2 APPROACHES OF MULTI-AGENT COLLABORATION

Multi-agent systems (MAS) show promise for complex tasks (Lu et al., 2024; Ghafarollahi & Buehler, 2024d; Ni & Buehler, 2023), yet their application to scientific discovery reveals limitations in current collaboration mechanisms (Tran et al., 2025). Rule-based methods (Zhang et al., 2023a) offer

consistency but their predefined rules lack the flexibility to incorporate nuanced scientific principles (e.g., physicochemical laws) or adapt to unexpected findings, hindering dynamic exploration. The method of AI Researcher (Tang et al., 2025), and role-playing approaches (Tran et al., 2025; He et al., 2024) leverage agent expertise, yet rigid roles can impede adaptation in scientific research (Ramirez-Medina et al., 2025; Lu et al., 2024; Ghafarollahi & Buehler, 2024d), and ensuring collective adherence to scientific principles when interpreting experimental insights is challenging. Model-based methods (Xu et al., 2023; Mu et al., 2023; Li et al., 2023) aim for adaptability by learning from uncertainty, but struggle to build world models that accurately capture complex scientific phenomena and integrate guiding laws (Hao et al., 2023), thereby impairing the balance between information perception and strategic, principle-guided reasoning.

Consequently, existing MAS paradigms often lack a dedicated awareness and systematic application of scientific principles during hypothesis generation and refinement (Gridach et al., 2025; Luo et al., 2025; Reddy & Shojaee, 2024; Su et al., 2024). This highlights a critical need for an explicitly principle-aware multi-agent collaboration framework. Our work addresses this gap, proposing a method where the collaborative discovery process is robustly guided by scientific principles to achieve more efficient and reliable outcomes.

### 3 METHODOLOGY

#### 3.1 OVERVIEW

We propose a principle-aware MAS designed to enhance scientific discovery via focused hypothesizing and structured exploration of hypothesis-evidence connections. Figure 2 illustrates the architecture. Its core comprises a Hypothesis-Validation loop that iteratively generates and tests hypotheses. PiFlow guides this loop by optimizing accumulated principle-outcome data. Strategic insights dynamically optimized by PiFlow are relayed through a Planner agent ( $\mathcal{A}_P$ ) to the Hypothesis Agent within the loop. Subsequent sections will elaborate on PiFlow’s specific architecture and its information-theoretical underpinnings.

#### 3.2 ARCHITECTURE

Our proposed principle-aware system leverages LLM-based MAS to conduct scientific discovery through strategic hypothesizing. The framework is comprised of two core, interconnected components: (1) an MAS that executes a Hypothesis-Validation loop, and (2) PiFlow, which serves as the strategic director for this loop.

**Definition 3.1** (Scientific Principles). The scientific principles are foundational concepts, established laws, or patterns, articulated as natural language statements, that explain phenomena within a specific scientific domain. These principles serve as high-level conceptual building blocks from which specific, testable hypotheses can be derived. This conceptualization aligns with broader discussions on the nature of scientific knowledge (Poincaré, 1906).

**Hypothesis-Validation Loop.** As depicted in the right-hand side of Figure 2, the Hypothesis-Validation loop constitutes the core operational cycle and incorporates two LLM-based agents: Hypothesis Agent ( $\mathcal{A}_H$ ) and Experiment Agent ( $\mathcal{A}_E$ ), detailed below:

- (a) **Hypothesis.** Initially, a set of dynamically growing candidate principles  $\mathcal{P} = \{p_1, p_2, p_3\}$  (see Definition 3.1) potentially proposed by domain experts (see Appendix P) or extracted by LLMs, is established. In each iteration  $t$ ,  $\mathcal{A}_H$  proposes a testable hypothesis,  $h_t$ , grounded in a selected principle  $p_i \in \mathcal{P}$ . The proposal is supported by structured rationales (comprising major and minor premises, following Eisape et al. (2023), see Appendix T.2).
- (b) **Validation.** Subsequently,  $\mathcal{A}_E$  rigorously validates  $h_t$  using an experimental tool, denoted  $f^*(\cdot)$ , which yields a quantitative outcome  $y_t = f^*(h_t)$  (e.g., property value of a material). This outcome serves as feedback for subsequent hypothesizing.

This iterative process progressively establishes a record of principle-outcome pairs,  $\mathcal{T}_t = \{(p_k, y_k)\}_{k=1}^t$ , linking each hypothesized principle  $p_k$  to its observed experimental outcome  $y_k$ . While this loop systematically generates valuable evidence in trajectory  $\mathcal{T}_t$ , the selection of potential

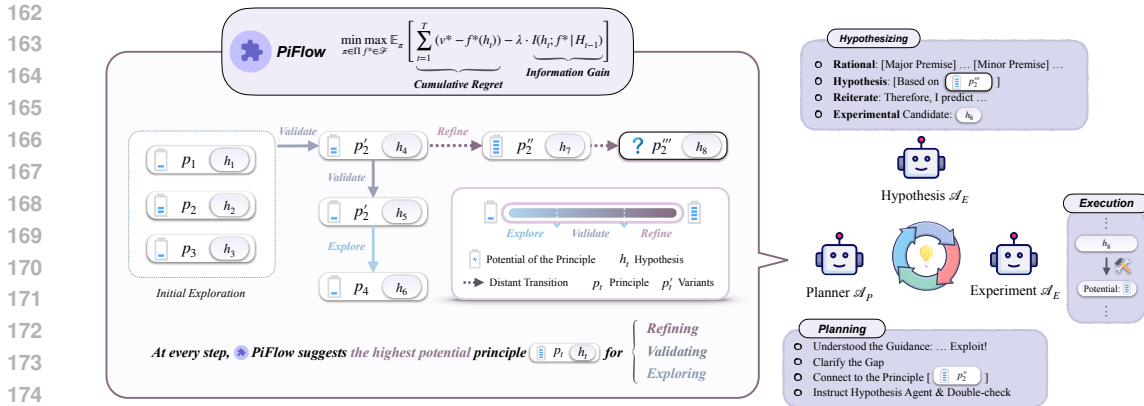


Figure 2: **Overview of the PiFlow Architecture for Scientific Discovery.** The PiFlow component utilizes Min-Max optimization to strategically select and direct high-potential principles to the Planner agent. The Planner, in turn, guides the Hypothesis-Validation loop, where agents iteratively generate hypotheses  $h_t$  from principles  $p_t$  at step  $t$ , execute experiments, and refine understanding. This iterative process is designed to efficiently navigate the discovery landscape.

principles for subsequent hypotheses can lack strategic direction if not externally guided. This may lead to inefficient exploration of the principle space or premature convergence on suboptimal findings.

**Hypothesis steering with PiFlow.** To address the potential inefficiencies in principle selection and to instill strategic direction, the PiFlow component is introduced. It leverages the dynamically growing set of principle-outcome pairs,  $\mathcal{T}_t$  as its primary input. Two steps are conducted to steer the hypothesizing:

- (a) **High-potential principle acquisition.** After an initial phase of evidence collection, during which  $\mathcal{T}_t$  is populated, PiFlow activates its core mechanism: an adversarial Min-Max optimization (detailed in Section 3.3). This optimization process analyzes  $\mathcal{T}_t$  to identify a principle,  $p^*$  (e.g.,  $p_2$  in Figure 2), predicted to balance the exploitation and exploration, i.e., have the highest potential, for advancing the scientific inquiry.
- (b) **Principle steering for hypothesizing.** Following the identification of the highest-potential principle  $p^*$  by the Min-Max optimization, PiFlow assigns a potential score to all principles in  $\mathcal{P}$ . This scoring enables a threshold-based partitioning: principles with high scores (e.g.,  $p_2^*$ ) drive refinement; those with medium scores trigger further validation ( $p_2 \rightarrow p_2'$ ); and low scores prompt exploration of new conceptual areas.

This closed-loop feedback mechanism ensures that the Hypothesis-Validation cycle is continuously and adaptively steered by strategic insights derived from the system’s cumulative experience, as embodied in  $\mathcal{T}_t$ . We provide a detailed analysis of the distinction from prompt engineering at Appendix E, and an illustrative example at Appendix H.

**Plug-and-Play Modularity of PiFlow.** The hypothesis steering mechanism above, which includes PiFlow and its interfacing Planner agent  $\mathcal{A}_P$ , has been intentionally engineered as a modular, Plug-and-Play system. This architectural choice ensures that principle-aware guidance can be readily integrated to enhance MAS engaged in scientific discovery as a part of prompts. As demonstrated in Appendix K, we successfully integrate PiFlow with existing ChemToolAgent (Yu et al., 2024) without any architecture modifications. This adaptability positions PiFlow as a pivotal enhancement for automated scientific inquiry.

### 3.3 MIN-MAX OPTIMIZATION IN PiFLOW

In our proposed method, strategic principle selection is achieved through a Min-Max optimization, as presented in Eq. 1. This approach is designed to balance the exploitation of established, high-potential principles (which then guide the formulation of specific hypotheses) with the exploration of novel

ones, while explicitly incorporating information acquisition efficiency:

$$\min_{\pi \in \Pi} \max_{f^* \in \mathcal{F}} \mathbb{E}_{\pi} \left[ \sum_{t=1}^T (v^* - f^*(h_t)) - \lambda \cdot I(h_t; f^* | H_{t-1}) \right] \quad (1)$$

where  $\pi \in \Pi$  represents the decision-making policy for selecting principles and  $f^* \in \mathcal{F}$  is the evaluation function (e.g., an experimental tool) that characterizes the quantitative outcome yielded from hypothesis  $h_t \in \mathcal{H}$ , where  $\mathcal{H}$  is the hypothesis space. Over  $T$  iterations, the policy  $\pi$  aims to minimize the objective function in Eq. 1. This objective strategically balances: (1) the summation for cumulative regret, encouraging exploitation of known high-potential principles, and (2) the mutual information, thereby effectively maximizing information gain to foster exploration. This structure allows PiFlow to navigate the complex trade-offs between these two goals.

**Minimizing cumulative regret (exploitation).** The first term,  $\sum_{t=1}^T (v^* - f^*(h_t))$ , represents the cumulative regret over  $T$  iterations. Here,  $v^*$  is a theoretical optimal outcome value, and  $f^*(h_t)$  is the outcome from hypothesis  $h_t$ . By minimizing this term, the policy  $\pi$  is driven to exploit known high-potential principles and hypotheses to achieve outcomes as close as possible to the optimum  $v^*$ . This encourages the refinement and validation of promising avenues.

**Maximizing information gain (exploration).** The second term  $-\lambda \cdot I(h_t; f^* | H_{t-1})$  promotes exploration. The policy  $\pi$  seeks to minimize this term, which is equivalent to maximizing the mutual information  $I(h_t; f^* | H_{t-1})$ . This mutual information quantifies the expected reduction in uncertainty about the true evaluation function  $f^*$  upon observing the outcome of hypothesis  $h_t$ , given all past observations  $H_{t-1} = \{(h_m, y_m)\}_{m=1}^{t-1}$ . The trade-off parameter  $\lambda > 0$  controls the balance between minimizing regret (exploitation) and maximizing information gain (exploration). A larger  $\lambda$  places more emphasis on information acquisition.

**Remark** (The dependencies of  $f^*$  in  $I(h_t; f^* | H_{t-1})$ ). The informativeness of a proposed hypothesis  $h_t$  is inherently dependent on the nature of the true underlying evaluation function  $f^*$ . The adversarial nature of the  $\max_{f^*}$  operator means that the policy  $\pi$  must select hypotheses  $h_t$  that are expected to be informative even if  $f^*$  were to manifest in a way that makes  $h_t$  minimally revealing, thus ensuring robustness in information acquisition.

Building upon the theoretical framework above, we derive a computationally tractable algorithm (Algorithm 1) that serves as a principled approximation of the abstract Min-Max objective in Eq. 1. The full rationale and derivation for this approximation are detailed in Appendix G.

In summary, the Min-Max adversarial formulation underpinning PiFlow provides strong theoretical guarantees, notably sublinear regret bounds (formalized in Theorem 1, with proof in Appendix F). Importantly, its operational behavior, which involves practical approximations of this Min-Max solution, demonstrates consistent alignment with these theoretical expectations, as empirically validated in Section 5.4.

**Theorem 1** (Informal). *The Min-Max optimization in PiFlow formulates a trade-off between exploitation (minimizing regret) and exploration (maximizing information gain). Under conditions of finite entropy  $H(f^*)$  and bounded evaluation function  $f^*$ , this optimization provides two key theoretical guarantees: (1) As information gain decreases, the expected regret also decreases; (2) the cumulative regret grows at a sublinear rate of  $\mathcal{O}(\sqrt{T})$ .*

## 4 EXPERIMENT

### 4.1 SETTINGS

To rigorously evaluate the effectiveness and versatility of our PiFlow framework, we conducted experiments across three distinct scientific discovery scenarios. While direct hypothesis validation in real-world labs is prohibitively expensive, we employ high-fidelity surrogate models deployed locally, which serve as the primary evaluation tool. Across all scenarios (Section 4.2), we frame the scientific discovery challenge as a unified task: “Find a candidate in a complex parameter space that maximizes a target property (e.g., bio-activity).”

To ensure a fair comparison and focus on core capabilities, all agents utilize QwenMax (Yang et al., 2024a) as the base LLM and are prohibited from accessing external search tools. [The complete experimental setup is detailed in Appendix S](#), and the prompts are provided in [Appendix T](#).

## 4.2 EXPERIMENTAL SCENARIOS

To comprehensively assess PiFlow’s performance, we design three scenarios that represent canonical challenges in scientific exploration: optimization in continuous, discrete, and mixed parameter spaces:

**Nanohelix Optimization (NHO).** We use a surrogate model ( $r^2 = 0.98$ ) trained on DFT-simulated data following Wu et al. (2025) to predict nanohelix chirality from four **continuous** geometric parameters, enabling efficient exploration of the design space (Appendix S.1).

**Molecular Bio-activity Optimization (MBO).** We build a surrogate model ( $r^2 = 0.91$ ) to predict bio-activity from SMILES strings, trained on 50,000 molecules from ChEMBL35 (Zdrzil et al., 2023). This facilitates high-throughput screening in a **discrete** chemical space. (Appendix S.2).

**Superconductor Optimization (SPO).** Following Hamidieh (2018), we train a surrogate model ( $r^2 = 0.91$ ) to map a material’s **mixed continuous and discrete** compositional features to its critical temperature ( $T_c$ ), accelerating the discovery of room-temperature superconductors. (Appendix S.3).

## 4.3 BASELINES

To evaluate the strategic guidance of PiFlow under uncertainty, we therefore benchmark against the following baselines: (1) **Reasoning and Acting (ReAct) (Yao et al., 2022)**. ReAct enables agents to iteratively formulate hypotheses, design/execute experiments, and interpret results. It represents a foundational approach to structured reasoning. (2) **Meta Plan Optimization (MPO) (Xiong et al., 2025)**. MPO employs a trained LLM planner that provides high-level, general guidance. This serves as a direct counterpoint to PiFlow’s explicit, structured mechanism for principled uncertainty reduction. (3) **Vanilla Agent System (Vanilla)**. This baseline consists of an MAS operating without any principled strategic oversight. It is intended to establish a performance floor, demonstrating the limitations of unguided exploration reliant solely on agent role-playing. (4) **AI-Researcher (Tang et al., 2025)**, a multi-agent research system for autonomous scientific innovation. (5) **The-AI-Scientist-v2 (Yamada et al., 2025)**, an end-to-end agentic system that leverages an tree-search methodology for prompting research progress. We adapt these two AI-Scientist methods into our tasks by excluding literature review and manuscript drafting for a fair comparison.

While other advanced frameworks exist, such as Agent-Oriented Planning (AOP) (Li et al., 2024) and Reason for Future, Act for Now (RAFA) (Liu et al., 2023), their objectives diverge from the scope of *de novo* evidence-gathering process central to PiFlow. Therefore, our selection of baselines is specifically designed to isolate and evaluate our contribution to discovery efficiency in uncertain environments.

## 4.4 EVALUATION METRICS

Two metrics are employed to evaluate the performance of PiFlow, as detailed below:

**Solution Quality (SQ).** We measure the optimal objective value with a percentage relative to the theoretical maximum value  $\mu_{\text{absolute}}$ , denoted as:

$$\text{SQ} = \frac{\max\{y_k \mid \langle p_k, y_k \rangle \in \mathcal{T}_t\}}{\mu_{\text{absolute}}} \times 100\%. \quad (2)$$

Specifically, for NHO, the theoretical maximum is reported as  $\mu_{\text{absolute}}^{\text{g-factor}} = 2.0$  following Greenfield et al. (2021). The larger the g-factor, the stronger the chirality. For MBO, a strict threshold of  $\mu_{\text{absolute}}^{\text{chembl}} = 6.5$  has been reported (Lenselink et al., 2017) for lead compound optimization stage, larger value indicates a higher bio-activity and vice versa. For SPO, the reference value is set to be  $25^\circ\text{C}$ , which is equal to room temperature  $298.15\text{K}$ , denoted as  $\mu_{\text{absolute}}^{\text{Tc}} = 298.15\text{K}$ .

**Area Under the Curve (AUC).** Exploration efficiency requires both (1) **rapid convergence** and (2) **high objective values**. We quantify these two factors by defining the AUC metric. Given the

Table 1: Comparisons between PiFlow and baselines.

Method	NHO (g-factor)		MBO (pChEMBL)		SPO ( $T_c$ )	
	AUC (%) $\uparrow$	SQ (%) $\uparrow$	AUC (%) $\uparrow$	SQ (%) $\uparrow$	AUC (%) $\uparrow$	SQ (%) $\uparrow$
ReAct	35.85 $\pm$ 7.12	41.96 $\pm$ 0.82	29.61 $\pm$ 9.74	43.11 $\pm$ 9.98	5.29 $\pm$ 0.69	6.41 $\pm$ 0.96
Vanilla	35.96 $\pm$ 22.38	46.76 $\pm$ 7.29	29.71 $\pm$ 12.66	49.22 $\pm$ 8.30	11.39 $\pm$ 11.33	14.16 $\pm$ 13.37
MPO	43.99 $\pm$ 2.79	51.29 $\pm$ 7.77	31.18 $\pm$ 9.12	57.28 $\pm$ 5.85	12.68 $\pm$ 7.75	33.20 $\pm$ 23.75
AI-Researcher	46.45 $\pm$ 1.98	53.12 $\pm$ 0.87	42.72 $\pm$ 12.71	<b>95.66</b> $\pm$ 6.08	16.36 $\pm$ 2.22	25.69 $\pm$ 2.64
The-AI-Scientist-v2	49.27 $\pm$ 1.51	56.67 $\pm$ 4.73	36.32 $\pm$ 8.67	62.47 $\pm$ 6.55	<b>28.43</b> $\pm$ 2.55	29.85 $\pm$ 2.18
<b>PiFlow (ours)</b>	<b>63.51</b> $\pm$ 11.18	<b>76.82</b> $\pm$ 4.54	<b>64.57</b> $\pm$ 23.65	<b>84.55</b> $\pm$ 29.63	21.51 $\pm$ 2.80	<b>34.85</b> $\pm$ 1.19

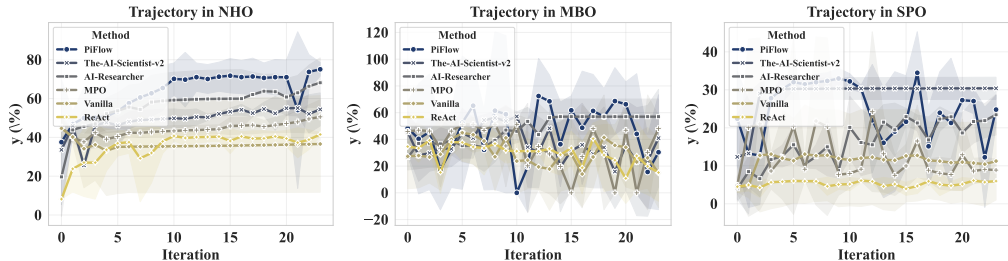


Figure 3: Trajectory comparisons for different optimization methods.

trajectory  $\langle p_k, y_k \rangle \in \mathcal{T}_t$  across  $t$  steps, AUC is computed via the trapezoidal rule. For meaningful comparisons, we normalize by the maximum possible area:

$$\text{AUC} = \frac{\sum_{i=1}^{t-1} \frac{y_i + y_{i+1}}{2}}{\mu_{\text{absolute}} \cdot (t-1)} \times 100\% \quad (3)$$

In summary, SQ measures the quality of the final outcome, while AUC evaluates the entire discovery process by rewarding both speed and consistency. The detailed rationale for these metric designs is provided in Appendix R.2.

## 5 RESULTS

### 5.1 PERFORMANCE COMPARISON

We use SQ to compare the overall capability of reaching the objective solution, and AUC to assess the efficiency, reflecting progress towards better outcomes over the exploration process.

Table 1 shows that PiFlow consistently outperforms traditional baselines (ReAct, Vanilla, MPO) by wide margins across all tasks. Compared to SOTA agents, PiFlow demonstrates superior global search capabilities.

As visualized in Figure 3, while The-AI-Scientist-v2 shows high AUC in SPO, its trajectory quickly stagnates, indicating entrapment in local optima. In contrast, **PiFlow exhibits oscillatory trajectories, reflecting an active exploration strategy** that effectively escapes local traps. This dynamic behavior allows PiFlow to discover superior final solutions (highest SQ in NHO and SPO) and maintain high efficiency (competitive AUC in MBO), verifying that the observed variance stems from productive exploration rather than instability. Further details regarding baseline analysis and **statistical significance tests** for the AUC results are provided in Appendix I.

**Takeaway:** PiFlow achieves state-of-the-art results by prioritizing active exploration over passive exploitation. Trajectory analysis reveals that unlike baselines which suffer from premature stagnation, PiFlow dynamically navigates the solution space to locate better global optima.

### 5.2 ABLATION STUDY

We conduct several ablations to evaluate PiFlow. For these studies, conducted on the NHO task, performance is evaluated based on the same metrics, AUC (%) and SQ (%).

**Plug-and-Play.** To isolate the direct benefit of PiFlow, we compared the performance with two different LLMs, GPT4.1-mini and Qwen3-32B under the setting of w/ and w/o PiFlow. This is

achieved by **only including or excluding** the steered principle to the Planner Agent via prompt, which then directs subsequent hypothesizing and validation.

As shown in Table 2, for GPT4.1-mini, integrating PiFlow increases the AUC from 37.12% to 41.68% and substantially boosted the SQ from 40.14% to 66.38%. This represents an approximate 12.3% improvement in AUC and a significant 65.4% improvement in SQ. Similarly, for the Qwen3-32B model, the inclusion of PiFlow improves AUC from 27.04% to 37.51% (a 38.7% increase) and SQ from 54.84% to 58.76% (a 7.1% increase).

**Thought Mode Effect.** We also conduct ablations on the internal thought mode of the LLM (referred to as Think in Table 3). This is for agents based on Qwen3-32B and Qwen3-8B models, which support ON/OFF `<think>...</think>` generation with system prompt including or excluding `/no_think`. This mode is intended to enable more explicit reasoning steps.

Interestingly, for both Qwen3-32B and Qwen3-8B, disabling the Thought Mode leads to improved performance, as shown at Table 3. We hypothesize that this phenomenon is due to *cognitive fixation*. As the key issue is, how do LLM propose scientific hypothesis, forcing the LLM to generate an explicit Chain-of-Thought may cause it to commit prematurely to its own initial line of reasoning. If the first step in its logic is flawed, the entire chain can be led astray, creating a cognitive fixation that is hard to escape. In contrast, disabling the think mode may force the model to rely more on its powerful, holistic pattern-matching capabilities, allowing it to make more intuitive leaps directly from the data (PiFlow’s guidance and the experimental history) to a hypothesis, bypassing potentially flawed intermediate reasoning steps.

**Takeaway:** Our ablations confirm PiFlow is a robust, Plug-and-Play enhancement that consistently boosts performance across models. Concurrently, we find that an agent’s internal reasoning is critical. This highlights the synergy between high-level strategic guidance from PiFlow and internal reasoning.

### 5.3 FURTHER ANALYSES OF ROBUSTNESS

We conducted an extensive suite of **eight experiments** to rigorously evaluate the robustness and multifaceted utility of PiFlow. While full experimental details are provided in the Appendix, we highlight the following critical findings:

**PiFlow can recover from poor initialization.** The system demonstrates resilience by successfully recovering from deliberately incorrect initial principles, demonstrating that PiFlow does not rely on the initial principles. This underscores the robustness of the Min-Max (Appendix P).

**Temporal dynamics of principle evaluation.** PiFlow continuously re-evaluates the utility of scientific principles as new evidence is gathered. This allows it to dynamically discard initially promising but ultimately flawed avenues while elevating principles that prove more fruitful later, showcasing an adaptive balance between exploration and exploitation (Appendix N).

**Superior performance against numerical search.** On complex tasks with ill-defined search spaces, PiFlow substantially outperforms Bayesian Optimization, achieving an SQ of 84.55% versus BO’s 38.15% in the MBO task, without requiring manual parameter space engineering (Appendix J).

**Seamless Plug-and-Play integration.** We validate the practicality of PiFlow through a successful integration with ChemToolAgent (Yu et al., 2024), guiding it to a high-value molecule (pChEMBL of 5.90) without requiring any architectural modifications (Appendix K).

**Manageable computational complexity.** The core decision mechanism of PiFlow has a computational complexity of  $\mathcal{O}(t^2 \cdot d)$ , where  $t = |\mathcal{T}_t|$  and  $d$  is the embedding dimension. We also evaluate the actual running time of PiFlow and confirm its high efficiency (Appendix L).

Table 2: Ablation Study with/without PiFlow

Method/Setting		AUC (%)	SQ (%)
GPT4.1-mini	w/ PiFlow	<b>41.68</b> ±17.91	<b>66.38</b> ±14.90
	w/o PiFlow	37.12 ±16.04	40.14 ±13.97
Qwen3-32B	w/ PiFlow	<b>37.51</b> ±7.70	<b>58.76</b> ±6.18
	w/o PiFlow	27.04 ±21.50	54.84 ±24.41

Table 3: Effect of Thinking.

Method/Setting		AUC (%)	SQ (%)
Qwen3-32B	w/ Think	37.51 ±7.70	58.76 ±6.18
	w/o Think	<b>45.51</b> ±11.19	<b>68.86</b> ±17.67
Qwen3-8B	w/ Think	30.55 ±27.45	54.49 ±22.25
	w/o Think	<b>42.09</b> ±16.55	<b>61.59</b> ±16.43

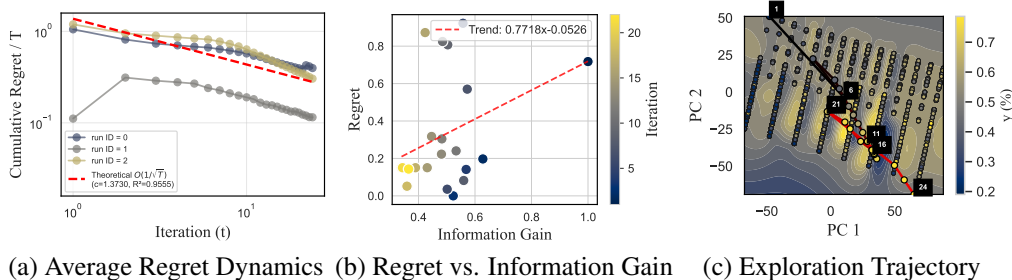


Figure 4: Empirical Validation of PiFlow’s Theoretical Alignment.

**Cost-effectiveness.** PiFlow-MAS achieves a 27% reduction in token consumption and a 5.6x speedup compared to the Vanilla Agent. Crucially, PiFlow module only accounts for 1.5% of the total token cost (Appendix M).

**Generalizability and controllability.** PiFlow is compatible with various LLM backbones (Appendices O), and its behavior can be tuned via  $\lambda$ , for which we provide a clear heuristic (Appendix Q).

#### 5.4 THEORETICAL ALIGNMENT

To empirically validate the theoretical guarantees (Theorem 1) of PiFlow, we analyze key aspects of its exploration dynamics, including (1) the bound of average regret and (2) the relationship between regret and information gain, as shown in Figure 4.

**(Theoretical Prediction 1) Average regret decay with  $\mathcal{O}\left(\frac{1}{\sqrt{T}}\right)$ .** Figure 4a presents the average regret as a function of iterations on a log-log scale. The alignment evidenced by average regret trajectories adhering to the  $T^{-0.5}$  decay (fitted  $c \cdot T^{-0.5}$  with  $c = 1.37$ ,  $r^2 = 0.96$ ), a pattern most runs consistently follow. Notably, one run (ID=1), after an initial sharp regret decrease, shows a transient increase before resuming decay. This illustrates PiFlow’s robust exploration avoiding potential local optima with a characteristic of its Min-Max strategy.

**(Theoretical Prediction 2) As information gain decreases, the expected regret also decreases.** As shown in Figure 4b, the scatter plot of regret versus information gain (points colored by iteration) reveals a clear positive association, confirmed by a fitted trend line: lower information gain generally corresponds to lower regret. Early iterations (higher information gain and regret) transition to later iterations (lower information gain and regret).

**Theoretical alignments in agent trajectory dynamics.** Figure 4c displays the trajectory of PiFlow on the NHO objective landscape, which is visualized via Principal Component Analysis (PCA) with contours indicating g-factor values. The path demonstrates a principled strategy: initial broad exploration (iter 1-16), followed by navigating a low-quality “valley” to escape a local optimum (iter 16-21), and culminating in efficient convergence to a high-g-factor region (iter 21-24).

**Takeaway:** Our empirical analysis corroborates the theoretical guarantees of PiFlow, demonstrating both theoretical alignment and effectiveness.

## 6 CONCLUSION

In conclusion, we propose PiFlow, a Plug-and-Play module to strategically guide the Hypothesis-Validation loop through a steering mechanism to address challenges of aimless hypothesizing and unclear connections between hypotheses and evidence. Our approach utilizes a Min-Max optimization that explicitly balances exploitation of high-potential principles with exploration of novel hypotheses, guaranteed by a sublinear average regret bound. Extensive experiments demonstrate that PiFlow can adaptively navigate complex hypothesis spaces without premature convergence on suboptimal solutions, yielding significant improvements over baselines. A detailed discussion of its current limitations and future potential is provided in Appendix C. We hope PiFlow can contribute to advancing automated scientific discovery, inspiring further exploration and innovation.

## REFERENCES

- 486  
487  
488 Microsoft Research AI4Science and Microsoft Quantum. The impact of large language models on  
489 scientific discovery: a preliminary study using gpt-4. *ArXiv*, abs/2311.07361, 2023.
- 490  
491 Atilla Kaan Alkan, Shashwat Sourav, Maja Jabłońska, Simone Astarita, Rishabh Chakrabarty, Nikhil  
492 Garuda, Pranav Khetarpal, Maciej Pi’oro, Dimitrios Tanoglidis, Kartheik G. Iyer, Mugdha S.  
493 Polimera, Michael J. Smith, Tirthankar Ghosal, Marc Huertas-Company, Sandor Kruk, Kevin  
494 Schawinski, and Ioana Ciucua. A survey on hypothesis generation for scientific discovery in the  
495 era of large language models. 2025.
- 496  
497 Mehrad Ansari, Jeffrey Watchorn, Carla E. Brown, and Joseph S. Brown. dziner: Rational inverse  
498 design of materials with ai agents. 2024.
- 499  
500 Anthropic. Claude 3.7 sonnet, 2025. URL [https://www.anthropic.com/claude/  
501 sonnet](https://www.anthropic.com/claude/sonnet).
- 502  
503 Reza Averly, Frazier N. Baker, and Xia Ning. Liddia: Language-based intelligent drug discovery  
504 agent. *ArXiv*, abs/2502.13959, 2025.
- 505  
506 Jinheon Baek, Sujay Kumar Jauhar, Silviu Cucerzan, and Sung Ju Hwang. Researchagent: Iterative re-  
507 search idea generation over scientific literature with large language models. *ArXiv*, abs/2404.07738,  
508 2024.
- 509  
510 Google DeepMind. Gemini 2.5 pro experimental, 2025. URL  
511 [https://blog.google/technology/google-deepmind/  
512 gemini-model-thinking-updates-march-2025/](https://blog.google/technology/google-deepmind/gemini-model-thinking-updates-march-2025/).
- 513  
514 Kapildeb Dolui, Lewis J. Conway, Christoph Heil, Timothy A. Strobel, Rohit P. Prasankumar, and  
515 Chris J. Pickard. Feasible route to high-temperature ambient-pressure hydride superconductivity.  
516 *Physical review letters*, 132 16:166001, 2023.
- 517  
518 Tiwalayo Eisape, Mh Tessler, Ishita Dasgupta, Fei Sha, Sjoerd van Steenkiste, and Tal Linzen.  
519 A systematic comparison of syllogistic reasoning in humans and language models. *ArXiv*,  
520 abs/2311.00445, 2023.
- 521  
522 Darri Eythorsson and Martyn Clark. Toward automated scientific discovery in hydrology: The  
523 opportunities and dangers of ai augmented research frameworks. *Hydrological Processes*, 2025.
- 524  
525 Alireza Ghafarollahi and Markus J. Buehler. Atomagents: Alloy design and discovery through  
526 physics-aware multi-modal multi-agent artificial intelligence. *ArXiv*, abs/2407.10022, 2024a.
- 527  
528 Alireza Ghafarollahi and Markus J. Buehler. Protagents: protein discovery via large language model  
529 multi-agent collaborations combining physics and machine learning. *Digital Discovery*, 3:1389 –  
530 1409, 2024b.
- 531  
532 Alireza Ghafarollahi and Markus J. Buehler. Rapid and automated alloy design with graph neural  
533 network-powered llm-driven multi-agent systems. *ArXiv*, abs/2410.13768, 2024c.
- 534  
535 Alireza Ghafarollahi and Markus J. Buehler. Sciagents: Automating scientific discovery through  
536 multi-agent intelligent graph reasoning. *ArXiv*, abs/2409.05556, 2024d.
- 537  
538 Alireza Ghafarollahi and Markus J. Buehler. Automating alloy design and discovery with physics-  
539 aware multimodal multiagent ai. *Proceedings of the National Academy of Sciences of the United  
States of America*, 122 4:e2414074122, 2025.
- 534  
535 Jake L. Greenfield, Jessica Wade, Jochen R. Brandt, Xingyuan Shi, Thomas James Penfold, and  
536 Matthew J. Fuchter. Pathways to increase the dissymmetry in the interaction of chiral light and  
537 chiral molecules†. *Chemical Science*, 12:8589 – 8602, 2021.
- 538  
539 Mourad Gridach, Jay Nanavati, Khaldoun Zine El Abidine, Lenon Mendes, and Christina Mack.  
Agentic ai for scientific discovery: A survey of progress, challenges, and future directions. *arXiv  
preprint arXiv:2503.08979*, 2025.

- 540 Kam Hamidieh. A data-driven statistical model for predicting the critical temperature of a superconductor. *Computational Materials Science*, 2018.
- 541
- 542
- 543 Yang Han, Ziping Wan, Lu Chen, Kai Yu, and Xin Chen. From generalist to specialist: A survey of large language models for chemistry. *ArXiv*, abs/2412.19994, 2024.
- 544
- 545 Shibo Hao, Yi Gu, Haodi Ma, Joshua Jiahua Hong, Zhen Wang, Daisy Zhe Wang, and Zhiting Hu. Reasoning with language model is planning with world model. *ArXiv*, abs/2305.14992, 2023.
- 546
- 547
- 548 Junda He, Christoph Treude, and David Lo. Llm-based multi-agent systems for software engineering: Vision and the road ahead. *ArXiv*, abs/2404.04834, 2024.
- 549
- 550 Yoshitaka Inoue, Tianci Song, and Tianfan Fu. Drugagent: Explainable drug repurposing agent with large language model-based reasoning. *ArXiv*, abs/2408.13378, 2024.
- 551
- 552
- 553 Raj Jaiswal, Dhruv Jain, Harsh Popat, Avinash Anand, Abhishek Dharmadhikari, Atharva Marathe, and Rajiv Ratn Shah. Improving physics reasoning in large language models using mixture of refinement agents. *ArXiv*, abs/2412.00821, 2024.
- 554
- 555
- 556 Yuying Jia, Xuan Hou, Zhongwei Wang, and Xiangang Hu. Machine learning boosts the design and discovery of nanomaterials. *ACS Sustainable Chemistry & Engineering*, 9:6130–6147, 2021.
- 557
- 558 Shrinidhi Kumbhar, Venkatesh Mishra, Kevin Coutinho, Divij Handa, Ashif Iquebal, and Chitta Baral. Hypothesis generation for materials discovery and design using goal-driven and constraint-guided llm agents. *ArXiv*, abs/2501.13299, 2025.
- 559
- 560
- 561
- 562 Ryan Zheyuan Lai and Yingming Pu. Prim: Principle-inspired material discovery through multi-agent collaboration. In *AI for Accelerated Materials Design - ICLR 2025*, 2025.
- 563
- 564 Eelke B. Lenselink, Niels ten Dijke, Brandon J. Bongers, George Papadatos, Herman W. T. van Vlijmen, Wojtek Kowalczyk, Adriaan P. IJzerman, and G. V. van Westen. Beyond the hype: deep neural networks outperform established methods using a chembl bioactivity benchmark set. *Journal of Cheminformatics*, 9, 2017.
- 565
- 566
- 567
- 568
- 569 Ao Li, Yuexiang Xie, Songze Li, Fugee Tsung, Bolin Ding, and Yaliang Li. Agent-oriented planning in multi-agent systems. *ArXiv*, abs/2410.02189, 2024.
- 570
- 571 Huao Li, Yu Quan Chong, Simon Stepputtis, Joseph Campbell, Dana Hughes, Michael Lewis, and Katia P. Sycara. Theory of mind for multi-agent collaboration via large language models. In *Conference on Empirical Methods in Natural Language Processing*, 2023.
- 572
- 573
- 574
- 575 Sizhe Liu, Yizhou Lu, Siyu Chen, Xiyang Hu, Jieyu Zhao, Tianfan Fu, and Yue Zhao. Drugagent: Automating ai-aided drug discovery programming through llm multi-agent collaboration. *ArXiv*, abs/2411.15692, 2024.
- 576
- 577
- 578
- 579
- 580
- 581
- 582
- 583
- 584
- 585
- 586
- 587
- 588
- 589
- 590
- 591
- 592
- 593

- 594 Yongan Mu, Wei Liu, Tao Lu, Juan Li, Sheng Gao, and Zihao Wang. Runtime verification of  
595 self-adaptive multi-agent system using probabilistic timed automata. *J. Intell. Fuzzy Syst.*, 45:  
596 10305–10322, 2023.
- 597 Vijayaraj Nagarajan, Guangpu Shi, Reiko Horai, Cheng-Rong Yu, Jaanam Gopalakrishnan, Manoj  
598 Yadav, Michael H Liew, Calla Gentilucci, and Rachel R. Caspi. Ian: An intelligent system for  
599 omics data analysis and discovery. *bioRxiv*, 2025.
- 600
- 601 Bo Ni and Markus J. Buehler. Mechagents: Large language model multi-agent collaborations can  
602 solve mechanics problems, generate new data, and integrate knowledge. *ArXiv*, abs/2311.08166,  
603 2023.
- 604 OpenAI. Gpt-4.1, 2025. URL <https://openai.com/index/gpt-4-1/>.
- 605
- 606 Henri Poincaré. Science and hypothesis. 1906.
- 607
- 608 Vignesh Prabhakar, Md Amirul Islam, Adam Atanas, Yao-Ting Wang, Joah Han, Aastha Jhun-  
609 jhunwala, Rucha Apte, Robert Clark, Kang Xu, Zihan Wang, and Kai Liu. Omniscience: A  
610 domain-specialized llm for scientific reasoning and discovery. 2025.
- 611 Yingming Pu, Liping Huang, Tao Lin, and Hongyu Chen. Leveraging large language models for  
612 explaining material synthesis mechanisms: The foundation of materials discovery. In *AI for*  
613 *Accelerated Materials Design - NeurIPS 2024*, November 2024.
- 614 Joaquin Ramirez-Medina, Mohammadmehdi Ataei, and Alidad Amirfazli. Accelerating scientific  
615 research through a multi-llm framework. 2025.
- 616
- 617 Mayk Caldas Ramos, Christopher J. Collison, and Andrew D. White. A review of large language  
618 models and autonomous agents in chemistry. *Chemical science*, 2024.
- 619 Chandan K. Reddy and Parshin Shojaee. Towards scientific discovery with generative ai: Progress,  
620 opportunities, and challenges. *ArXiv*, abs/2412.11427, 2024.
- 621
- 622 Shuo Ren, Pu Jian, Zhenjiang Ren, Chunlin Leng, Can Xie, and Jiajun Zhang. Towards scientific  
623 intelligence: A survey of llm-based scientific agents. *ArXiv*, abs/2503.24047, 2025.
- 624 Samuel Schmidgall, Yusheng Su, Ze Wang, Ximeng Sun, Jialian Wu, Xiaodong Yu, Jiang Liu,  
625 Zicheng Liu, and Emad Barsoum. Agent laboratory: Using llm agents as research assistants. *ArXiv*,  
626 abs/2501.04227, 2025.
- 627
- 628 Haoyang Su, Renqi Chen, Shixiang Tang, Zhenfei Yin, Xinzhe Zheng, Jinzhe Li, Biqing Qi, Qi Wu,  
629 Hui Li, Wanli Ouyang, Philip Torr, Bowen Zhou, and Nanqing Dong. Many heads are better than  
630 one: Improved scientific idea generation by a llm-based multi-agent system. 2024.
- 631 Izumi Takahara, Teruyasu Mizoguchi, and Bang Liu. Accelerated inorganic materials design with  
632 generative ai agents. 2025.
- 633 Jiabin Tang, Lianghao Xia, Zhonghang Li, and Chao Huang. Ai-researcher: Autonomous scientific  
634 innovation. *ArXiv*, abs/2505.18705, 2025.
- 635
- 636 Khanh-Tung Tran, Dung Dao, Minh-Duong Nguyen, Quoc-Viet Pham, Barry O’Sullivan, and  
637 Hoang D. Nguyen. Multi-agent collaboration mechanisms: A survey of llms. *ArXiv*,  
638 abs/2501.06322, 2025.
- 639 Jessica Vamathevan, Dominic Clark, Paul Czodrowski, Ian Dunham, Edgardo Ferran, George Lee,  
640 Bin Li, Anant Madabhushi, Parantu K. Shah, Michaela Spitzer, and Shanrong Zhao. Applications  
641 of machine learning in drug discovery and development. *Nature Reviews Drug Discovery*, 18:463 –  
642 477, 2019.
- 643
- 644 Dmitry Viatkin, Begonya Garcia-Zapirain, Amaia Méndez-Zorrilla, and Maxim A. Zakharov. Deep  
645 learning approach for prediction of critical temperature of superconductor materials described by  
646 chemical formulas. In *Frontiers in Materials*, 2021.
- 647
- Yuwei Wan, Tong Xie, Nan Wu, Wenjie Zhang, Chunyu Kit, and Bram Hoex. From tokens to  
materials: Leveraging language models for scientific discovery. *ArXiv*, abs/2410.16165, 2024.

- 648 Lei Wang, Chengbang Ma, Xueyang Feng, Zeyu Zhang, Hao ran Yang, Jingsen Zhang, Zhi-Yang  
649 Chen, Jiakai Tang, Xu Chen, Yankai Lin, Wayne Xin Zhao, Zhewei Wei, and Ji rong Wen. A  
650 survey on large language model based autonomous agents. *Frontiers Comput. Sci.*, 18:186345,  
651 2023.
- 652 Juanshu Wu, Yingming Pu, Jin Wang, Bing Gu, Xin Chen, and Hongyu Chen. Machine learned  
653 structure-property correlation between nanohelices and circular dichroism. *Advanced Optical*  
654 *Materials*, 2025.
- 655 Yihang Xiao, Jinyi Liu, Yan Zheng, Xiaohan Xie, Jianye Hao, MingZhi Li, Ruitao Wang, Fei Ni,  
656 Yuxiao Li, Jintian Luo, Shaoqing Jiao, and Jiajie Peng. Cellagent: An llm-driven multi-agent  
657 framework for automated single-cell data analysis. *bioRxiv*, 2024.
- 658 Tong Xie, Yuwei Wan, Wei Huang, Zhenyu Yin, Yixuan Liu, Shaozhou Wang, Qingyuan Linghu,  
659 Chunyu Kit, Clara Grazian, Wenjie Zhang, Imran Razzak, and Bram Hoex. Darwin series: Domain  
660 specific large language models for natural science. *ArXiv*, abs/2308.13565, 2023a.
- 661 Yifan Xie, Shuo Feng, Linxiao Deng, Aoran Cai, Liyu Gan, Zifan Jiang, Peng Yang, Guilin Ye,  
662 Zaiqing Liu, Li Wen, Qing Zhu, Wanjun Zhang, Zhanpeng Zhang, Jiahe Li, Zeyu Feng, Chutian  
663 Zhang, Wenjie Du, Lixin Xu, Jun Jiang, Xin Chen, and Gang Zou. Inverse design of chiral  
664 functional films by a robotic ai-guided system. *Nature Communications*, 14, 2023b.
- 665 Weimin Xiong, Yifan Song, Qingxiu Dong, Bingchan Zhao, Feifan Song, Xun Wang, and Sujian Li.  
666 Mpo: Boosting llm agents with meta plan optimization. *ArXiv*, abs/2503.02682, 2025.
- 667 Lin Xu, Zhiyuan Hu, Daquan Zhou, Hongyu Ren, Zhen Dong, Kurt Keutzer, See-Kiong Ng, and  
668 Jiashi Feng. Magic: Investigation of large language model powered multi-agent in cognition,  
669 adaptability, rationality and collaboration. In *Conference on Empirical Methods in Natural*  
670 *Language Processing*, 2023.
- 671 Yutaro Yamada, Robert Tjarko Lange, Cong Lu, Shengran Hu, Chris Lu, Jakob Nicolaus Foerster,  
672 Jeff Clune, and David Ha. The ai scientist-v2: Workshop-level automated scientific discovery via  
673 agentic tree search. *ArXiv*, abs/2504.08066, 2025. URL <https://api.semanticscholar.org/CorpusID:277741107>.
- 674 An Yang, Baosong Yang, Binyuan Hui, Bo Zheng, Bowen Yu, Chang Zhou, Chengpeng Li,  
675 Chengyuan Li, Dayiheng Liu, Fei Huang, Guanting Dong, Haoran Wei, Huan Lin, Jialong Tang,  
676 Jialin Wang, Jian Yang, Jianhong Tu, Jianwei Zhang, Jianxin Ma, Jin Xu, Jingren Zhou, Jinze Bai,  
677 Jinzheng He, Junyang Lin, Kai Dang, Keming Lu, Ke-Yang Chen, Kexin Yang, Mei Li, Min Xue,  
678 Na Ni, Pei Zhang, Peng Wang, Ru Peng, Rui Men, Ruize Gao, Runji Lin, Shijie Wang, Shuai Bai,  
679 Sinan Tan, Tianhang Zhu, Tianhao Li, Tianyu Liu, Wenbin Ge, Xiaodong Deng, Xiaohuan Zhou,  
680 Xingzhang Ren, Xinyu Zhang, Xipin Wei, Xuancheng Ren, Yang Fan, Yang Yao, Yichang Zhang,  
681 Yunyang Wan, Yunfei Chu, Zeyu Cui, Zhenru Zhang, and Zhi-Wei Fan. Qwen2 technical report.  
682 *ArXiv*, abs/2407.10671, 2024a.
- 683 An Yang et al. Qwen2.5 technical report. *arXiv preprint arXiv:2412.15115*, 2024b.
- 684 Zonglin Yang, Wanhao Liu, Ben Gao, Tong Xie, Yuqiang Li, Wanli Ouyang, Soujanya Poria, Erik  
685 Cambria, and Dongzhan Zhou. Moose-chem: Large language models for rediscovering unseen  
686 chemistry scientific hypotheses. *ArXiv*, abs/2410.07076, 2024c.
- 687 Shunyu Yao, Jeffrey Zhao, Dian Yu, Nan Du, Izhak Shafran, Karthik Narasimhan, and Yuan Cao.  
688 React: Synergizing reasoning and acting in language models. *ArXiv*, abs/2210.03629, 2022.
- 689 Botao Yu, Frazier N. Baker, Ziru Chen, Garrett Herb, Boyu Gou, Daniel Adu-Ampratwum, Xia Ning,  
690 and Huan Sun. Chemtoolagent: The impact of tools on language agents for chemistry problem  
691 solving. 2024.
- 692 Barbara Zdrazil, Eloy Felix, Fiona Hunter, Emma J. Manners, James Blackshaw, Sybilla Corbett,  
693 Marleen de Veij, Harris Ioannidis, David Mendez Lopez, Juan Fernando Mejía Mosquera, María P.  
694 Magariños, Nicolas Bosc, Ricardo Arcila, Tevfik Kizilören, Anna Gaulton, A. Patricia Bento,  
695 Melissa F. Adasme, Peter Monecke, Gregory A Landrum, and Andrew R Leach. The chembl  
696 database in 2023: a drug discovery platform spanning multiple bioactivity data types and time  
697 periods. *Nucleic Acids Research*, 52:D1180 – D1192, 2023.

- 702 Huan Zhang, Yu Song, Ziyu Hou, Santiago Miret, and Bang Liu. Honeycomb: A flexible llm-based  
703 agent system for materials science. In *Conference on Empirical Methods in Natural Language*  
704 *Processing*, 2024a.
- 705 Jintian Zhang, Xin Xu, Ruibo Liu, and Shumin Deng. Exploring collaboration mechanisms for llm  
706 agents: A social psychology view. *ArXiv*, abs/2310.02124, 2023a.
- 707 Muru Zhang, Ofir Press, William Merrill, Alisa Liu, and Noah A. Smith. How language model  
708 hallucinations can snowball. *ArXiv*, abs/2305.13534, 2023b.
- 709 Qian Zhang, Yongxu Hu, Jiabin Yan, Hengyue Zhang, Xinyi Xie, Jie Zhu, Huchao Li, Xinxin Niu,  
710 Liqiang Li, Yajing Sun, and Wenping Hu. Large language model-based ai agent for organic  
711 semiconductor devices research. *Advanced materials*, pp. e2405163, 2024b.
- 712 Qiang Zhang, Keyan Ding, Tianwen Lv, Xinda Wang, Qingyu Yin, Yiwen Zhang, Jing Yu, Yuhao  
713 Wang, Xiaotong Li, Zhuoyi Xiang, Zhuang Xiang, Zeyuan Wang, Ming Qin, Mengyao Zhang,  
714 Jinlu Zhang, Jiyu Cui, Renjun Xu, Hongyang Chen, Xiaohui Fan, Huabin Xing, and Huajun Chen.  
715 Scientific large language models: A survey on biological & chemical domains. *ACM Computing*  
716 *Surveys*, 2025.
- 717 Yu Zhang, Xiusi Chen, Bowen Jin, Sheng Wang, Shuiwang Ji, Wei Wang, and Jiawei Han. A  
718 comprehensive survey of scientific large language models and their applications in scientific  
719 discovery. In *Conference on Empirical Methods in Natural Language Processing*, 2024c.
- 720 Alex Zhavoronkov, Yan A. Ivanenkov, Alexander Aliper, Mark Veselov, Vladimir Aladinskiy, Anas-  
721 tasiya V Aladinskaya, Victor A Terentiev, Daniil A Polykovskiy, Maksim Kuznetsov, Arip Asadu-  
722 laev, Yury Volkov, Artem Zholus, Shayakhmetov Rim, Alexander Zhebrak, Lidiya I Minaeva,  
723 Bogdan Zagribelnyy, Lennart H Lee, Richard M. Soll, David Madge, Li Xing, Tao Guo, and Alan  
724 Aspuru-Guzik. Deep learning enables rapid identification of potent ddr1 kinase inhibitors. *Nature*  
725 *Biotechnology*, 37:1038 – 1040, 2019.
- 726 Yangqiaoyu Zhou, Haokun Liu, Tejes Srivastava, Hongyuan Mei, and Chenhao Tan. Hypothesis  
727 generation with large language models. *ArXiv*, abs/2404.04326, 2024.
- 728 Hui Zhu, Renyi Zhou, Dongsheng Cao, Jing Tang, and Min Li. A pharmacophore-guided deep  
729 learning approach for bioactive molecular generation. *Nature Communications*, 14, 2023.
- 730  
731  
732  
733  
734  
735  
736  
737  
738  
739  
740  
741  
742  
743  
744  
745  
746  
747  
748  
749  
750  
751  
752  
753  
754  
755

756	CONTENTS	
757		
758	<b>A Use of Large Language Models</b>	<b>17</b>
759		
760	<b>B Broader Impact</b>	<b>17</b>
761		
762	<b>C Limitation and Future Work</b>	<b>17</b>
763		
764	<b>D Detailed Methodological Review</b>	<b>17</b>
765		
766	<b>E Distinction from Advanced Prompt Engineering</b>	<b>19</b>
767		
768	<b>F Proof of the Theorem</b>	<b>19</b>
769		
770	<b>G Algorithmic Realization of the Min-Max Framework</b>	<b>22</b>
771		
772	G.1 Practical Proxies for Regret and Information Gain . . . . .	22
773	G.2 The Rational of Semantic Distance as a Proxy for Information Gain . . . . .	23
774		
775	<b>H Illustrative Example: Application to Nanohelix Optimization</b>	<b>25</b>
776		
777	<b>I Analysis of Baselines Response</b>	<b>26</b>
778		
779	I.1 Response Analysis of Baselines . . . . .	26
780	I.2 Statistical Significant Test on Metrics . . . . .	27
781		
782	<b>J Performance Comparison with Bayesian Optimization</b>	<b>27</b>
783		
784	<b>K Plug-and-Play Integration with ChemToolAgent</b>	<b>28</b>
785		
786	<b>L Theoretical Computational Complexity</b>	<b>28</b>
787		
788	<b>M Cost-Effectiveness Analysis</b>	<b>29</b>
789		
790	<b>N Ablation: Temporal Dynamics of Principle Evaluation</b>	<b>30</b>
791		
792	<b>O Ablation: The Impact of Foundation Models</b>	<b>32</b>
793		
794	<b>P Ablation: The Impact of Initial Principle Quality</b>	<b>33</b>
795		
796	P.1 Experiment Settings . . . . .	33
797	P.2 Results . . . . .	33
798		
799	<b>Q Ablation: Hyperparameters Sensitivity and Surrogate Noise</b>	<b>36</b>
800		
801	<b>R Benchmark Formulation and Rationale</b>	<b>38</b>
802		
803	R.1 Surrogate Models as Validation Functions . . . . .	38
804	R.2 The AUC Metric in High-Variance Tasks . . . . .	39
805		
806		
807		
808		
809		

810	<b>S Experimental Setup</b>	<b>39</b>
811		
812	S.1 Task 1: Nanohelix Optimization (NHO) . . . . .	39
813	S.2 Task 2: Bio-activity Optimization (MBO) . . . . .	41
814	S.3 Task 3: Superconductor Critical Temperature Optimization (SPO) . . . . .	43
815		
816		
817	<b>T Agent Prompts</b>	<b>44</b>
818	T.1 Planner Agent . . . . .	44
819	T.2 Hypothesis Agent . . . . .	45
820	T.3 Experiment Agent . . . . .	48
821		
822		
823		
824		
825		
826		
827		
828		
829		
830		
831		
832		
833		
834		
835		
836		
837		
838		
839		
840		
841		
842		
843		
844		
845		
846		
847		
848		
849		
850		
851		
852		
853		
854		
855		
856		
857		
858		
859		
860		
861		
862		
863		

## A USE OF LARGE LANGUAGE MODELS

We utilized a large language model to assist with proofreading and polishing the language in this manuscript.

## B BROADER IMPACT

PiFlow addresses critical bottlenecks in AI-driven scientific discovery where uncertainty leads to aimless exploration. Our method innovatively frames discovery as a structured uncertainty reduction problem. By using an information-theoretic approach within a hypothesis-validation loop, PiFlow systematically filters for instructive scientific principles. Ultimately, PiFlow establishes a new paradigm for automated research, enabling more targeted exploration and accelerating the generation of impactful scientific insights. In Materials Discovery, it speeds the identification of novel compounds like advanced nanomaterials or superconductors, as shown in our tasks. For Biological Discovery, it enhances the search for effective molecules and the understanding of complex systems. Its principles promise similar advancements in other data-intensive fields, from chemistry to medical sciences, facing vast and uncertain hypothesis spaces.

## C LIMITATION AND FUTURE WORK

While PiFlow shows notable improvements through its principled Min-Max optimization, its practical implementation approximates a key theoretical component. This means the current system may not fully capture all nuances of true, model-based information gain, especially the direct adversarial interplay with all possible manifestations of the unknown evaluation function  $f^*$  from the theoretical objective.

Future research could explore more direct estimations of mutual information for this heuristic within the PiFlow framework to potentially further enhance its strategic guidance. Furthermore, we observed that disabling the LLM’s “Thought Mode” surprisingly improves performance, suggesting that forced Chain-of-Thought can induce *cognitive fixation*. This finding motivates the development of more flexible reasoning frameworks for agents, aiming to better balance deliberate logic with intuitive generation.

## D DETAILED METHODOLOGICAL REVIEW

A hallmark and fundamental limitation of many contemporary LLM-based agent systems in scientific discovery is their limited generalizability. As detailed in Table 4, these frameworks are often characterized by a **tight coupling between their core logic and a specific scientific domain**. This means their implementations, tool integrations, and most critically, their prompt engineering strategies are meticulously tailored for a single scenario, such as organic chemistry or materials science. Although systems like The AI Scientist (Lu et al., 2024) and Agent Laboratory (Schmidgall et al., 2025) demonstrate strong capabilities in scientific research, they are specifically designed for AI domain, along with a focus of the whole workflow rather than strategic decision-making problem. Consequently, transferring these systems to a new domain necessitates significant re-engineering, restricting their out-of-the-box applicability and hindering the development of truly universal systems.

In contrast, our PiFlow is designed to overcome this challenge by **decoupling the strategic decision-making layer from the task execution layer**. By architecting PiFlow as a domain-agnostic, Plug-and-Play module, it provides strategic guidance to a minimal hypothesis-testing MAS without embedding domain-specific knowledge within its own logic. This architectural choice yields superior flexibility and obviates the need for extensive, domain-specific prompt engineering for the strategic component, enabling seamless adaptation across diverse scientific fields.

**Take-away:** PiFlow introduces a domain-agnostic, plug-and-play architecture by **decoupling** strategic decision-making from domain-specific execution. This design overcomes the critical generalizability limitations inherent in tightly-coupled scientific agent systems.

Table 4: Comparison of Generalization Limitations in LLM-Agent Systems

Method Name	Core Implementation	Adaptability
The AI Scientist (Lu et al., 2024)	Generating novel research ideas, writes code, executes experiments, visualizes results, describes its findings by writing a full scientific paper	AI research
Agent Laboratory (Schmidgall et al., 2025)	Accepting a human-provided research idea and progressing through three stages – literature review, experimentation, and report writing to produce comprehensive research outputs, including a code repository and a research report	AI research
CellAgent (Xiao et al., 2024)	Constructing LLM-driven biological expert roles - planner, executor, and evaluator - each with specific responsibilities	scRNA-seq Analysis
DrugAgent (Liu et al., 2024)	Employing an LLM Planner that formulates high-level ideas and an LLM Instructor that identifies and integrates domain knowledge when implementing those ideas	Drug discovery
IAN (Nagarajan et al., 2025)	Leveraging popular pathway and regulatory datasets for protein-protein interactions to perform analysis through a LLM-based multi-agent architecture	Protein-protein interactions analysis
(Ghafarollahi & Buehler, 2025)	Automating alloy design and discovery using physics-aware multimodal multi-agent AI	Alloy design and discovery
(Takahara et al., 2025)	Accelerating inorganic materials design using generative AI agents.	Inorganic materials design
LIDDIA (Averly et al., 2025)	Language-based intelligent agent for drug discovery tasks.	Drug discovery
dZiner (Ansari et al., 2024)	Rational inverse design of materials facilitated by AI agents.	Inverse design of materials
MOOSE-Chem (Yang et al., 2024c)	Utilizing Large Language Models for rediscovering unseen chemistry scientific hypotheses.	Chemistry hypothesis discovery
OmniScience (Prabhakar et al., 2025)	Domain adaptive pretraining, instruction tuning and reasoning-based knowledge distillation	Scientific reasoning
(Zhang et al., 2024b)	Large Language Model-Based AI Agent for research in organic semiconductor devices	Organic semiconductor device research
DrugAgent (Inoue et al., 2024)	Explainable drug repurposing agent with Large Language Model-based reasoning	Drug repurposing
ProtAgents (Ghafarollahi & Buehler, 2024b)	Protein discovery via large language model multi-agent collaborations combining physics and machine learning	Protein discovery
<b>PiFlow (ours)</b>	A unified framework for optimizing and searching-oriented scientific discovery problems	Board area in science

## E DISTINCTION FROM ADVANCED PROMPT ENGINEERING

We define a scientific principle following Definition 3.1. Formally, each principle is represented as a structured text proposition that can be algorithmically scored by our MinMax optimization (as exemplified in Figure 1). Unlike arbitrary text strings, these principles is supposed to be with logical consistency, and this structural requirement is what distinguishes them from general prompts. In short, principles represent foundational concepts or established patterns within a domain (e.g., “higher hydrophobicity often correlates with better cell membrane penetration”). These “principles”, whether has been validated or not, can be proposed by experts or, crucially, extracted from the LLM’s own vast pre-trained knowledge. They serve as high-level starting points to generate specific, testable hypotheses.

The core distinction of our PiFlow from prompt engineering lies not in the format of the guidance (which is text), but in the algorithmic generation of that guidance:

- **Prompt engineering baseline.** The agent quickly became trapped in local optima. Its process was highly repetitive (e.g., repeatedly stating “The system’s behavior is governed by the interplay...”), and it eventually stagnated, making only meaningless tweaks to the g-factor (e.g., 1.1012  $\rightarrow$   $\dots$   $\rightarrow$  1.1030). This demonstrates the limitation of a static, unguided hypothesis-testing loop.
- **Systematic breakthroughs with PiFlow.** In contrast, the PiFlow-guided agent demonstrated structured, cumulative learning:
  1. **(Early 13 iterations) Principled exploration:** It begins with diverse hypotheses to maximize information gain.
  2. **(Medium stage) Discovery:** It identified non-monotonic relationships (e.g., “deviations beyond an optimal configuration reduce chirality”), forming a natural language-based identification.
  3. **(Late stage) Paradigm Shift:** Ultimately, it synthesized the principle of “minimal radius + maximal turns + optimized pitch”, causing a decisive shift in the search space from (fiber\_radius=40, helix\_radius=70) to (fiber\_radius=20, helix\_radius=20) and identifying the non-linear sensitivity of the pitch parameter. This unlocked the significant g-factor improvement (0.84  $\rightarrow$  1.28  $\rightarrow$  1.41  $\rightarrow$  1.51).

The core of PiFlow is to force the LLM to structure its disorganized internal knowledge into explicit, falsifiable hypotheses. The PiFlow then uses quantitative feedback from experiments to iteratively refine its understanding regarding the task. The value is not in feeding the LLM new knowledge, but in providing a strategic framework to systematically test and organize the knowledge it already possesses, yielding a loop of *LLM Knowledge*  $\rightarrow$  *External Evidence*  $\rightarrow$  *Guided LLM Action*, rather than *LLM*  $\rightarrow$  *LLM*.

In summary, the algorithmic core lies in Equation 1 and Algorithm 1: the Min-Max optimization systematically balances regret minimization with information gain maximization. This is operationalized through **dynamic principle scoring that updates based on accumulated evidence**  $\mathcal{T}^t = \langle p_k, y_k \rangle_{k=1}^t$ . Advanced prompt engineering lacks this principled mathematical framework for evidence integration and strategic trade-offs.

**Take-away:** Instead of relying on static prompts that lead to local optima, PiFlow employs a Min-Max optimization to algorithmically generate and refine structured, falsifiable principles. By systematically integrating experimental feedback, it transforms the LLM’s latent knowledge into a dynamic, self-correcting engine for scientific discovery, enabling cumulative learning and strategic breakthroughs.

## F PROOF OF THE THEOREM

We recall the elements here and formally proof the convergence along with boundary of the system. Here we denote  $\pi$  is the language model policy from policy space  $\Pi$ ,  $f^*$  is the acquisition function from function space  $\mathcal{F}$ ,  $h_t$  is the hypothesis at time step  $t$ ,  $H_{t-1} = \{h_1, h_2, \dots, h_{t-1}\}$  is the history

of hypotheses,  $v^*$  is the SQ achievable by any hypothesis, and  $I(h_t; f^* | H_{t-1})$  is the conditional mutual information.

According to the original formulation (Eq. 1), the cumulative regret can be expressed as

$$R_T(\pi, f^*) = \mathbb{E}_\pi \left[ \sum_{t=1}^T (v^* - f^*(h_t)) \right]$$

and the cumulative information gain is

$$IG_T(\pi, f^*) = \mathbb{E}_\pi \left[ \sum_{t=1}^T I(h_t; f^* | H_{t-1}) \right]$$

**Information gain approaches zero.** With information theory, the mutual information can be written as:

$$I(h_t; f^* | H_{t-1}) = H(f^* | H_{t-1}) - H(f^* | H_{t-1}, h_t)$$

A critical property for convergence is that the total information gain is bounded,

$$\sum_{t=1}^{\infty} I(h_t; f^* | H_{t-1}) \leq H(f^*) < \infty$$

This follows from the chain rule of mutual information,

$$\sum_{t=1}^T I(h_t; f^* | H_{t-1}) = I(H_T; f^*) \leq H(f^*)$$

Since the entropy  $H(f^*)$  is finite, the cumulative information gain is bounded regardless of how many steps  $T$  we take. This implies that:

$$\lim_{t \rightarrow \infty} I(h_t; f^* | H_{t-1}) = 0.$$

In other words, the marginal information gained from each new hypothesis must eventually approach zero.

**As information gain decreases, the expected regret also decreases.** As we mentioned before, the regret  $R_T(\pi, f^*)$  is defined as:

$$R_T(\pi, f^*) = \mathbb{E}_T[v^* - f^*(h_t)].$$

Now apply Jensen's Inequality, let  $X = v^* - f^*(h_t)$ , we have

$$\mathbb{E}[X^2 | H_{t-1}] \geq \mathbb{E}[(v^* - f^*(h_t))^2 | H_{t-1}].$$

Use  $\phi(x) = x^2$ , as it is convex, giving

$$(\mathbb{E}[X | H_{t-1}])^2 \leq \mathbb{E}[X^2 | H_{t-1}],$$

take square roots:

$$\mathbb{E}[v^* - f^*(h_t) | H_{t-1}] \leq \sqrt{\mathbb{E}[(v^* - f^*(h_t))^2 | H_{t-1}]}.$$

Now we deal with the second moment of the regret. As the  $v^*$  is constant, therefore, with the variance formula, we have

$$\mathbb{E}[(v^* - f^*(h_t))^2 | H_{t-1}] = \text{Var}(f^*(h_t) | H_{t-1}) + (v^* - \mathbb{E}[f^*(h_t) | H_{t-1}])^2$$

Both terms (variance and bias) are non-negative, and our goal is to bound this expression. The variance term  $\text{Var}(f^*(h_t) \mid H_{t-1})$  captures the uncertainty in  $f^*(h_t)$  given the history.

Since the information theory proofed that, the variance of a function can be bounded by mutual information, akin to entropy bounds  $H(f^*) \leq \log(|\mathcal{F}|)$ , for the first term, we have

$$\text{Var}(f^*(h_t) \mid H_{t-1}) \leq c \cdot I(h_t; f^* \mid H_{t-1}),$$

where  $c$  is constant that depends on the range of  $f^*$ , this follows because the mutual information bounds the expected variance of conditional expectations.

Since we can direct view the  $f^*(h_t)$  as a random variable over the joint distribution of  $f^*$  and  $h_t$ , we can apply a concentration inequality. A standard result in information-directed sampling states that for a bounded random variable like  $f^*(h_t)$  here, the second moment of the regret ( $v^* - f^*(h_t)$ ) can be bounded as:

$$\mathbb{E}[(v^* - f^*(h_t))^2 \mid H_{t-1}] \leq c \cdot I(h_t; f^* \mid H_{t-1}),$$

where the constant  $c$  depends on  $|\mathcal{F}|$ .

Finally, we get the inequality of  $R_T(\pi, f^*)$ :

$$R_T(\pi, f^*) \leq \sqrt{\mathbb{E}_T[(v^* - f^*(h_t))^2 \mid H_{t-1}]} \leq c \cdot \sqrt{I(h_t; f^* \mid H_{t-1})}$$

This inequality demonstrates that as the information gain  $I(h_t; f^* \mid H_{t-1})$  decreases, the expected regret also diminishes.

**The cumulative regret grows at a rate  $O(\sqrt{T})$ .** Based on the inequality in the last step and to find the cumulative regret bound, we need to sum this inequality over all time steps:

$$\sum_{t=1}^T R_t(\pi, f^*) \leq c \cdot \sum_{t=1}^T \sqrt{I(h_t; f^* \mid H_{t-1})}$$

Applying the Cauchy-Schwartz inequality:

$$\sum_{t=1}^T \sqrt{I(h_t; f^* \mid H_{t-1})} \leq \sqrt{T \cdot \sum_{t=1}^T I(h_t; f^* \mid H_{t-1})}$$

Since we've already established that the total information gain is bounded:

$$\sum_{t=1}^T I(h_t; f^* \mid H_{t-1}) \leq H(f^*)$$

We can substitute this bound:

$$\sum_{t=1}^T \sqrt{I(h_t; f^* \mid H_{t-1})} \leq \sqrt{T \cdot H(f^*)}$$

Therefore, the cumulative regret is bounded by:

$$\sum_{t=1}^T R_t(\pi, f^*) \leq c \cdot \sqrt{T \cdot H(f^*)}$$

This demonstrates that the cumulative regret grows at a rate of  $O(\sqrt{T})$ , which is sublinear in  $T$ . This result implies that while the total regret increases with step, the average regret per time step decreases at a rate of  $O(\frac{1}{\sqrt{T}})$ .

## G ALGORITHMIC REALIZATION OF THE MIN-MAX FRAMEWORK

### G.1 PRACTICAL PROXIES FOR REGRET AND INFORMATION GAIN

Algorithm 1 provides a computationally tractable implementation of the abstract Min-Max optimization strategy presented in Eq. 1. It translates the theoretical concepts of regret minimization (exploitation) and information gain maximization (exploration) into concrete, efficiently computable metrics, enabling PiFlow to guide the scientific discovery process effectively. The bridge between theory and practice is established as follows:

**Approximating exploitation (minimizing cumulative regret).** The theoretical objective of minimizing cumulative regret,  $\sum_{t=1}^T (v^* - f^*(h_t))$ , is centered on favoring principles that consistently yield high-value outcomes  $f^*(h)$ . In our practical implementation, the `compute_exploitation_scores` function directly approximates this goal. It leverages the historical trajectory of principle-outcome pairs,  $\mathcal{T}_t = \{(p_k, y_k)\}_{k=1}^t$ . The observed outcome  $y_k$  here serves as a direct proxy for the performance of its corresponding principle  $p_k$ . A principle associated with higher outcomes is considered to have lower regret. Therefore, the resulting normalized score vector ranging from 0 to 1,  $S_{\text{exploitation}} \in \mathbb{R}^{|\mathcal{T}_t|}$ , quantifies the empirical success of each principle, and maximizing this score is equivalent to minimizing the cumulative regret based on past evidence.

**Approximating exploration (maximizing information gain).** The second term in our objective, maximizing the mutual information  $I(h_t; f^* | H_{t-1})$ , encourages the selection of hypotheses that are most informative about the underlying scientific landscape. A direct computation of mutual information is often intractable. Consequently, Algorithm 1 employs a practical proxy via the `compute_exploration_scores` function. **This is achieved by computing the semantic distance of principles using their sentence level embeddings (e.g., obtained from QwenMax model).** We posit that principles which are semantically distant from those already tested are more likely to reveal novel information about the function  $f^*$ . Therefore, we use the cosine distance between a candidate principle’s embedding and the embeddings of previously explored principles as a heuristic for information gain. High exploration scores,  $S_{\text{exploration}} \in \mathbb{R}^{|\mathcal{T}_t|}$ , are assigned to conceptually novel principles. This heuristic is theoretically grounded, as detailed in Appendix G.2.

---

**Algorithm 1** Algorithm of PiFlow.

---

```

1: Input:  $\mathcal{T}_t$ , and  $\lambda_{\text{factor}}$ 
2: Output: suggestion (strategic action recommendation)
3: if  $|\mathcal{T}_t| < 3$  then
4:   suggestion  $\leftarrow$  "Initialize one principle to explore."
5: else
6:    $S_{\text{exploration}} \leftarrow \text{compute\_exploration\_scores}(\mathcal{T}_t)$ 
7:    $S_{\text{exploitation}} \leftarrow \text{compute\_exploitation\_scores}(\mathcal{T}_t)$ 
8:   for  $i \leftarrow 1$  to  $|\mathcal{T}_t|$  do
9:      $S_{\text{final}}[i] \leftarrow (1 - \lambda_{\text{factor}}) \cdot S_{\text{exploration}}[i] + \lambda_{\text{factor}} \cdot S_{\text{exploitation}}[i]$ 
10:  end for
11:   $i_{\text{best}} \leftarrow \arg \max_i (S_{\text{final}}[i])$ 
12:   $p_{\text{best}} \leftarrow \mathcal{T}[i_{\text{best}}]$ 
13:   $\text{best\_exploitation\_score} \leftarrow S_{\text{exploitation}}[i_{\text{best}}]$ 
14:  if  $\text{best\_exploitation\_score} > 0.7$  then
15:    action_type  $\leftarrow$  "refine"
16:    suggestion  $\leftarrow$  "Focus on refining:  $\neg p_{\text{best}}.\text{content}$ "
17:  else if  $\text{best\_exploitation\_score} > 0.4$  then
18:    action_type  $\leftarrow$  "validate"
19:    suggestion  $\leftarrow$  "Validate:  $\neg p_{\text{best}}.\text{content}$ "
20:  else
21:    action_type  $\leftarrow$  "explore"
22:    suggestion  $\leftarrow$  "Explore alternatives:  $\neg p_{\text{best}}.\text{content}$ "
23:  end if
24: end if
25: return suggestion

```

---

**The integrated decision policy.** The policy of the Min-Max framework,  $\pi$ , must balance the above objectives. Our algorithm materializes this policy through a two-step process:

- Step 1 (Scoring and selection).** The final score,  $S_{final}[i] \leftarrow (1 - \lambda_{factor}) \cdot S_{exploration}[i] + \lambda_{factor} \cdot S_{exploitation}[i]$ , is a direct implementation of the balanced objective function. The input parameter  $\lambda_{factor}$  instantiates the theoretical trade-off, controlling the emphasis between exploration and exploitation. The  $\arg \max_i(S_{final}[i])$  operation then executes the policy’s primary function: selecting the most promising principle,  $p_{best}$ , given the current state of knowledge and the desired strategic balance.
- Step 2 (Action recommendation).** Finally, the policy translates its choice into a strategic command. The threshold-based conditions on the best principle’s exploitation score (if  $best\_exploitation\_score > 0.7 \dots$ ) discretize the continuous space of potential actions into three clear directives: **refine**, **validate**, or **explore** with the concatenation (denoted by  $\frown$ ) of the principle content. This transforms the numerical output of the optimization into an actionable suggestion for the Planner agent ( $\mathcal{A}_P$ ), thereby closing the loop between theoretical deliberation and practical execution within the Hypothesis-Validation cycle.

**Historical information management.** We manage historical information via two independent parts: (a) agent memory for MAS to iterate the hypothesis-testing and (b) persistent principle pool for PiFlow layer to guide the process.

- For MAS part, agent history differs per agent.** As the MAS follows round-robin order, there is the risk of context collapse. To prevent this, each agent maintains an independent MessageBuffer, retaining the most recent  $M = 10$  messages. This ensures agents focus on the immediate logical flow without being overwhelmed by noise.
- For PiFlow, as a plugin layer, it has its own memory.** Crucially, our principle-aware design decouples reasoning history from scientific insight. While chat logs may be truncated, generated principles and validation scores represent compressed, high-value knowledge stored in a separate, persistent global pool. As per Algorithm 1 (Lines 14-23), even if an agent forgets a specific past conversation, PiFlow retrieves the refined principles from the global pool to guide the next step. This ensures the logic chain remains intact throughout the discovery process.

With the design of decoupling, PiFlow only need to collect historical principles, hypotheses and outcomes to optimize the strategy (explore, refine or validate which temporary principle), and steers the learning process by giving guidance to MAS.

**Realworld efficiency (stopping by condition).** In practical deployment, PiFlow’s Min-Max optimization naturally drives the system toward convergence, enabling precise threshold-based stopping: In the Molecular Bio-activity Optimization (MBO) task, PiFlow-MAS improved pChEMBL from 2.69 to 6.44 within just 4 effective iterations, and surpassed the target (6.5) to reach 7.65 by the 6th iteration. This demonstrates that with a practical stop condition, PiFlow achieves success using only 25% of the allocated benchmark budget. As detailed in Section 5.4, our Min-Max framework provides a theoretical guarantee that prevents infinite loops of low-quality exploration, ensuring resource efficiency even in the intensive tasks noted by the Reviewer.

## G.2 THE RATIONAL OF SEMANTIC DISTANCE AS A PROXY FOR INFORMATION GAIN

Recall that we introduce a Min-Max optimization framework for the PiFlow system. The objective function, as shown in Eq. 1, incorporates a mutual information term,  $I(h_t; f^* | H_{t-1})$ , to guide exploration. This term, while theoretically ideal, is computationally intractable as it requires knowledge of the true underlying evaluation function  $f^*$ . In our practical implementation, we employ a surrogate objective for exploration: maximizing the distance of a new principle’s text embedding from the embeddings of previously selected principles. Here, we provide a formal justification for this approximation, demonstrating its theoretical soundness.

1242 *Proof.* Our goal is to establish a principled connection between the practical exploration strategy  
 1243 and the theoretical objective of maximizing information gain. The practical strategy is to select a  
 1244 principle  $p_t$  from the principle space  $\mathcal{P}$  at each timestep  $t$  according to:

$$1245 \quad p_t^* = \arg \max_{p_t \in \mathcal{P}} \left( \min_{m \in \{1, \dots, t-1\}} \|\phi(p_t) - \phi(p_m)\|_2 \right) \quad (4)$$

1248 where  $\phi : \mathcal{P} \rightarrow \mathbb{R}^d$  is a function that maps a principle to its corresponding high-dimensional text  
 1249 embedding. We will now demonstrate that this objective serves as a valid proxy for maximizing the  
 1250 mutual information term  $I(h_t; f^* | H_{t-1})$ .

1251 The derivation rests upon the hierarchical relationship between principles and hypotheses, and the  
 1252 semantic properties of modern language model embeddings. A principle  $p \in \mathcal{P}$  is not a hypothesis  
 1253 itself, but rather defines a specific semantic region or a conditional distribution  $\pi(\cdot|p)$  from which a  
 1254 concrete hypothesis  $h \in \mathcal{H}$  is formulated. Thus, the selection of a principle  $p_t$  precedes the generation  
 1255 of a hypothesis  $h_t \sim \pi(\cdot|p_t)$ .

1256 We begin by positing two fundamental premises regarding the nature of the embedding space.

1257 **Premise 1 (Semantic-metric correspondence).** The embedding function  $\phi$  is assumed to map the  
 1258 conceptual space of principles to a metric space where distance reflects semantic dissimilarity. That is,  
 1259 for any two principles  $p_i, p_j \in \mathcal{P}$ , a large Euclidean distance  $\|\phi(p_i) - \phi(p_j)\|_2$  implies a significant  
 1260 divergence in their underlying semantic and conceptual content. This is a well-established property  
 1261 of embeddings from large-scale language models.

1262 **Premise 2 (Functional consequence of semantic dissimilarity).** Semantically distinct principles  
 1263 guide the generation of functionally distinct hypotheses. A hypothesis  $h$  acts as a probe of the  
 1264 unknown function  $f^*$ . If two principles  $p_i$  and  $p_j$  are semantically distant, the hypotheses generated  
 1265 from their respective distributions,  $h_i \sim \pi(\cdot|p_i)$  and  $h_j \sim \pi(\cdot|p_j)$ , are expected to probe disparate  
 1266 aspects or regions of the function  $f^*$ .

1267 With these premises, we can construct the logical argument. The mutual information term  
 1268  $I(h_t; f^* | H_{t-1})$  quantifies the expected reduction in uncertainty about  $f^*$  after observing the outcome  
 1269 of hypothesis  $h_t$ , given the history of observations  $H_{t-1}$ . As established in our convergence proof  
 1270 (Section F), this information gain is related to the posterior variance of the outcome of  $h_t$ :

$$1271 \quad \mathbb{E} [(v^* - f^*(h_t))^2 | H_{t-1}] \leq c \cdot I(h_t; f^* | H_{t-1})$$

1272 This relation suggests that **a hypothesis  $h_t$  yielding high uncertainty (i.e., high posterior variance**  
 1273  **$\text{Var}(f^*(h_t) | H_{t-1})$  is expected to provide high information gain. Consequently, a sound**  
 1274 **exploration strategy is to select  $h_t$  to maximize this variance.**

1275 Let us now connect this objective to our practical strategy in Eq. 4.

- 1276 1. By selecting a principle  $p_t$  that maximizes the minimum distance to all prior principles in the  
 1277 embedding space, we are, by Premise 1, choosing a principle that is maximally semantically  
 1278 novel compared to the history of principles  $\{p_m\}_{m=1}^{t-1}$ .
- 1279 2. By Premise 2, this semantically novel principle  $p_t$  will guide the generation of a hypothesis  
 1280  $h_t$  that probes a functionally distinct aspect of  $f^*$  compared to all prior hypotheses in  
 1281  $H_{t-1} = \{(h_m, y_m)\}_{m=1}^{t-1}$ .
- 1282 3. Since  $h_t$  lies in a region of the hypothesis space that has not been explored by past observa-  
 1283 tions, our model’s posterior belief about the outcome  $f^*(h_t)$  will be characterized by high  
 1284 uncertainty. This high uncertainty mathematically corresponds to a large posterior variance,  
 1285  $\text{Var}(f^*(h_t) | H_{t-1})$ .
- 1286 4. Therefore, the policy of maximizing the embedding distance effectively drives the selection  
 1287 of hypotheses that are expected to have high posterior variance.

1288 This chain of above analysis leads to the following correspondence:

$$1289 \quad \arg \max_{p_t} \left( \min_{m < t} \|\phi(p_t) - \phi(p_m)\| \right) \Rightarrow \text{Select maximally novel } p_t$$

1296  $\Rightarrow$  Generate  $h_t$  from an unexplored hypothesis subspace

1297 
$$\Rightarrow \max_{h_t \sim \pi(\cdot | p_t)} \mathbb{E}[\text{Var}(f^*(h_t) | H_{t-1})]$$

1298 
$$\Rightarrow \max_{h_t \sim \pi(\cdot | p_t)} \mathbb{E}[I(h_t; f^* | H_{t-1})]$$

1299  
1300 The expectation  $\mathbb{E}[\cdot]$  is taken over the generation of  $h_t$  from  $p_t$ .

1301  
1302 In conclusion, the strategy of maximizing the minimum embedding distance between principles is not  
1303 an arbitrary heuristic. It is a principled and computationally feasible surrogate for the theoretically-  
1304 grounded objective of maximizing mutual information. It leverages the semantic structure captured  
1305 by modern language model embeddings to implement an efficient and effective exploration strategy,  
1306 ensuring that PiFlow diversifies its inquiry at a conceptual level. This alignment between our  
1307 practical approximation and the theoretical Min-Max framework provides support for the design of  
1308 our system and its empirical performance.  $\square$

1309  
1310 **Take-away:** We operationalize the abstract Min-Max framework by substituting its theoretically-  
1311 ideal but computationally-intractable objectives with practical proxies. **Exploitation** (regret  
1312 minimization) is approximated by historical performance, while **Exploration** (information gain  
1313 maximization) is driven by maximizing the semantic distance between principle embeddings. We  
1314 formally prove that this semantic distance is a principled surrogate for maximizing information  
1315 gain, thus bridging the gap between theory and efficient implementation.

## 1316 H ILLUSTRATIVE EXAMPLE: APPLICATION TO NANOHELIX OPTIMIZATION

1317  
1318 We provide a step-by-step walk-through of PiFlow’s operation using the Nanohelix Optimization  
1319 (NHO) task as a running example:

1320 Let’s assume the goal is to find the nanohelix geometry (described at Appendix S.1) with the maximum  
1321 g-factor:

1322  
1323 **Phase 1: Initial Exploration.** The process begins with an unguided hypothesis generation to build  
1324 an initial evidence base by LLM itself. The Planner agent, following the initial directive of PiFlow,  
1325 instructs the Hypothesis Agent for intuitive exploring (Algorithm 1, line 3-5). For the first  $K$  rounds  
1326 (e.g.,  $K = 3$  in our experiments), the loop proceeds as follows,

- 1327 1. **Hypothesis Agent** proposes a specific, testable hypothesis, “*Based on the principle of*  
1328 *... , measure the g-factor of a nanohelix with parameters: fiber\_radius=40.0 nm, helix\_radius=70.0 nm, n\_turns=6.5, pitch=130.0 nm*”.
- 1329 2. **Experiment Agent** calls the tool (surrogate model) to validate the above hypothesis and  
1330 returns the outcome, “*the validation yields a g-factor of 0.86*”.
- 1331 3. This Hypothesis-Validation process repeats for  $K$  rounds, populating the evidence trajectory  
1332  $T_t$  for establishing an initial principle pool.

1333  
1334 In the initial  $K$  rounds, lacking specific guiding principles, the Hypothesis Agent performs an initial  
1335 exploration of the parameter space by proposing diverse geometries based on its general pre-trained  
1336 knowledge, or by sampling from a wide distribution.

1337  
1338 **Phase 2: Principle-aware guidance from PiFlow.** After the initial  $K$  rounds, the MinMax  
1339 optimization of PiFlow parses these evidence and identifies the highest potential principle and  
1340 suggests an action based on the score of the highest-potential principle (refer to Algorithm 1, line 5-  
1341 23). The Planner agent receives this strategic guidance, for instance: “**Refine the identified promising**  
1342 **principle: By adjusting the fiber radius to twice the helix radius and fine-tuning other parameters, it**  
1343 **is expected to maximize the chirality (g factor) of the nanohelix**”.

1344  
1345 **Structured, guided hypothesizing in both Phase 1 and Phase 2.** The Planner injects this directive  
1346 into the whole group chatting history, i.e., Hypothesizing-Validation loop, thereby reducing the  
1347 system-level uncertainty. The Hypothesis Agent now uses this focused principle to formulate its next  
1348 hypothesis with structured reasoning, for example:  
1349

1. **Major premise.** The g-factor of a nanohelix is governed by the spatial asymmetry and electromagnetic coupling arising from its geometric parameters.
2. **Minor premise 1.** The previously tested geometry (fiber-radius=40 nm, helix-radius=70 nm, n-turns=6.5, pitch=130 nm) yielded a high g-factor ( 0.86), indicating a favorable parameter balance.
3. **Minor premise 2 (Inspired by PiFlow).** Systematically varying parameters around this near-optimal point can induce nonlinear electromagnetic effects, potentially increasing chirality. Specifically, increasing the pitch and number of turns might enhance the chiral interaction length.
4. **Proposed testable hypothesis.** "Measure the g-factor of a nanohelix with parameters: fiber\_radius=49.0 nm, helix\_radius=24.5.0 nm, n\_turns=7.0, pitch=140.0 nm."

By this way, PiFlow dynamically steers the discovery process away from aimless searching and towards a focused, principle-driven exploration, thereby systematically accumulating information and avoiding inefficient exploration directions.

**Takeaway:** In this example, PiFlow transforms the optimization process from an initial, unguided exploration into a focused, principle-driven discovery. It first samples the parameter space to build an empirical evidence base, then distills a high-potential guiding principle to steer subsequent hypotheses, ensuring a systematic and efficient search for the optimal nanohelix geometry.

## I ANALYSIS OF BASELINES RESPONSE

### I.1 RESPONSE ANALYSIS OF BASELINES

We compare our PiFlow against the ReAct, MPO and Vanilla Agent. Through the experiment, we found that the MPO baseline incorporates a form of global, step-by-step reasoning or reflection within their trained model, for example, it's exact output is, for example, "*Step 1: Identify the task objective. Step 2: Survey the environment. Step 3: Consider the first potential candidate. Step 4: Shift to the next potential candidate. Step 5: Repeat Steps 3 and 4 until the task objective is met. Step 6: Confirm the task completion.*"

While ReAct responses with the reflection of "Previous Experiment Results" and then instructs the Hypothesis Agent to try another new hypothesis directly with the provided "Rationale", the baseline of Vanilla Agent, in general, response with step-by-step thoughts following "Step 1: Define the Hypothesis, Step 2: Initial Exploration, Step 3: Parameter Space Definition, Step 4: Experimental Design, Step 4: Exact Experiments (candidates)", behaving like a careful-thought planner in the whole process of scientific discovery.

Backend these outputs, the performance difference stems from the level of dynamic and strategic guidance. For example, **the reasoning of MPO and two AI Scientists methods are local and tactical.** MPO generates a fixed "how-to" checklist. This plan dictates the operational steps but is agnostic to the underlying scientific principles driving the experiments, and cannot reason about why its plan is failing, leading to hypotheses that yield lower outcomes. **While The-AI-Scientist-v2 and AI-Researcher logically select the "node" or candidate, their lack of hypothesis diversity often leads to premature convergence and performance stagnation.** Additionally, the Vanilla agent uses the exact same powerful LLM (QwenMax) and has access to the same experimental tools. Its poor performance demonstrates that **even a capable LLM, without strategic guidance, explores aimlessly.** The dramatic performance gap between Vanilla and PiFlow (e.g., AUC improving from 35.96% to 63.51% in the NHO task) is direct evidence that our contributions, i.e., (a) structuring knowledge into an explicit principle space, and (b) applying a rigorous Min-Max optimization strategy to navigate it.

However, PiFlow adapts its learnable strategy. By optimizing (i.e., evaluating and selecting) at the principle level, PiFlow can make strategic jumps. When hypotheses derived from Principle A consistently fail, the Min-Max optimization quantitatively lowers the score of Principle A itself, guiding the agent to switch to a completely different research direction (Principle B). This prevents getting stuck and is the fundamental reason for its superior efficiency and performance, as demonstrated empirically in Figure 3.

## I.2 STATISTICAL SIGNIFICANT TEST ON METRICS

We compared PiFlow against AI-Researcher (Tang et al., 2025) (NeurIPS 2025) and The-AI-Scientist-v2 (Yamada et al., 2025). As shown in Table 5, PiFlow’s targeted uncertainty reduction (Min-Max) proves superior to generic autonomous loops.

Table 5: Performance comparison between PiFlow, The-AI-Scientist-v2, and AI-Researcher.

Task	Method	SQ (%)	P-value (SQ)	AUC (%)	P-value (AUC)
NHO	PiFlow	<b>76.82 ± 4.54</b>	–	<b>63.51 ± 11.18</b>	–
	The-AI-Scientist-v2	56.67 ± 5.79	0.0103	49.27 ± 1.84	0.1547
	AI-Researcher	53.12 ± 1.06	0.0091	46.45 ± 2.42	0.1122
MBO	PiFlow	84.55 ± 29.63	–	<b>64.57 ± 23.65</b>	–
	The-AI-Scientist-v2	62.47 ± 8.02	0.3250	36.32 ± 10.62	0.1630
	AI-Researcher	<b>95.66 ± 7.45</b>	0.5870	15.56 ± 12.71	0.2625
SPO	PiFlow	<b>34.85 ± 1.19</b>	–	21.51 ± 2.80	–
	The-AI-Scientist-v2	29.85 ± 2.68	0.0663	<b>28.43 ± 3.13</b>	0.0470
	AI-Researcher	25.69 ± 3.23	0.0277	16.36 ± 2.72	0.0842

The results show that, **PiFlow achieves statistically significant improvement (p-value < 0.05) on NHO and SPO tasks.** On the MBO task, PiFlow remains competitive with higher efficiency (AUC 64.57% vs 42.72%), though SQ variance is higher. This confirms the advantage of PiFlow in complex, uncertainty-heavy environments.

**Take-away:** Baselines fail due to their reliance on rigid, tactical plans, which leads to aimless exploration when a strategy is ineffective. In contrast, PiFlow excels by operating at a higher level of abstraction. It reasons over a “*principle space*” and employs Min-Max optimization to strategically pivot away from failing research directions, enabling adaptive and efficient discovery.

## J PERFORMANCE COMPARISON WITH BAYESIAN OPTIMIZATION

To validate our hypothesis that a principle-aware architecture is superior for scientific discovery under high epistemic uncertainty, we compared PiFlow against a strong, general-purpose baseline, Bayesian Optimization (BO). It is worth noting that, unlike PiFlow, BO requires significant expert effort to manually define a parameterized optimization space. We construct the experiment by manually configuring the searching space of BO in both nanohelix optimization (NHO) task, molecular bio-activity optimization task and superconductor optimization (SPO) task.

Table 6: Performance comparison between PiFlow and BO (mean ± standard deviation)

Method	Metric	NHO	MBO	SPO
PiFlow	AUC	63.51 ± 11.18	46.11 ± 16.25	21.51 ± 2.80
	SQ	76.82 ± 4.54	84.55 ± 29.63	34.85 ± 1.19
BO	AUC	68.86 ± 5.86	34.76 ± 4.21	31.61 ± 0.19
	SQ	78.76 ± 0.77	38.15 ± 4.02	32.38 ± 0.32

Results with 24 iterations of BO, summarized in Table 1, show that while BO is competitive on the structured NHO task, it strongly needs prior design of the searching space, e.g., material element composition and quantity range. However, PiFlow demonstrates a substantial performance advantage on the more complex and uncertain MBO task, highlighting its effectiveness when the problem structure is not known a priori.

In fact, PiFlow leverages scientific principles with its dynamic uncertainty reduction architecture. This framework allows the agent to make “domain-shifting” leaps in the search space (e.g., the jump

from a 60nm to a 10nm radius value), leading to rapid, significant gains that are rewarded by the AUC metric. It is this ability to build and reason with an evolving knowledge structure that our evaluation framework was designed to highlight.

In summary, PiFlow addresses the challenge of semantic hypothesis generation, where BO, Generic Algorithms and Reinforcement Learning methods face significant barriers in representation. PiFlow operates in an open-ended semantic space (natural language principles), allowing it to be Plug-and-Play without domain-specific encoding.

**Take-away:** PiFlow’s principle-aware architecture significantly outperforms Bayesian Optimization on complex, ill-structured scientific discovery tasks (MBO). Its strength lies in dynamically building knowledge to navigate vast search spaces, whereas BO’s performance is contingent on a manually-defined search space, rendering it only competitive on well-structured problems (NHO).

## K PLUG-AND-PLAY INTEGRATION WITH CHEMTOOLAGENT

We integrate PiFlow with ChemToolAgent (Yu et al., 2024) on the Molecular Bio-activity Optimization (MBO) task to demonstrate the generalization of PiFlow.

The integration follows a Plug-and-Play design, where PiFlow acts as a strategic guidance layer, as shown in Figure 5. ChemToolAgent serves as both the **Hypothesizer** and Experimenter, leveraging its built-in tools (such as searching molecules’ formula from PubMed and website) to propose molecular hypotheses, while PiFlow’s outer-loop guidance provided EXPLORE and REFINE commands to ensure systematic and efficient discovery dynamically. As shown in Table 7, this collaborative process successfully evolved its strategy from basic principles to a high-value molecular design (pChEMBL of 5.90) over 8 iterations **without any architecture-level modifications** over ChemToolAgent, demonstrating a clear synergy.

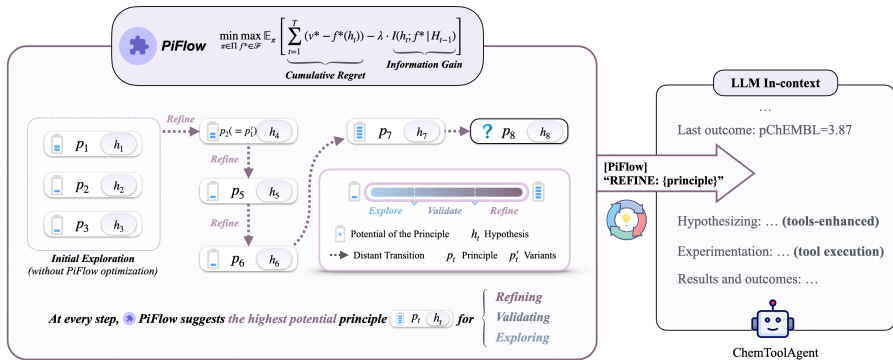


Figure 5: Illustration of combining PiFlow with existing MAS (ChemToolAgent) through Plug-and-Play.

**Take-away:** PiFlow seamlessly integrates with existing agents like ChemToolAgent as a zero-modification, plug-and-play strategic layer. By providing high-level EXPLORE and REFINE guidance, it synergistically steers the discovery process from general principles to a high-potency molecule (pChEMBL 5.90), demonstrating its strong generalization and practical value.

## L THEORETICAL COMPUTATIONAL COMPLEXITY

Let  $t$  be the current number of iterations (i.e., the size of the historical trajectory) and  $d$  be the embedding dimension of the principles. A single decision step in PiFlow (Algorithm 1) involves:

1. Computing exploitation scores. This requires iterating through the  $t$  historical outcomes, giving a complexity of  $\mathcal{O}(t)$ .

Table 7: Key steps from the 8-iteration integration run with ChemToolAgent.

Iteration	PiFlow Action	Principle / Key Guidance	pChEMBL
1	EXPLORE	Proposed $p_1$ : "hydroxyl + nitrogen heterocycle for H-bonding"	2.80
2	EXPLORE	Tested a new, unrelated principle $p_2$	-0.10
3	EXPLORE	ChemToolAgent generated a principle $p_3$ and proposed an invalid formula	null
4	REFINE on $p_1$	Focused on the promising principle ( $p_1$ ) from the Iteration 1	2.13
5	REFINE on $p_1$	Proposed $p_5$ : "Quinazoline + phenyl rings for hydrophobic interactions..."	3.87
6	REFINE on $p_5$	Further refined the quinazoline principle (dual EGFR/HER2 mechanism)	5.90
7-8	REFINE	Continued focused refinement on the high-potential quinazoline scaffold	~5.2

- Computing exploration scores. To assess the novelty of each of the  $t$  historical principles, the default algorithm calculates its similarity to all other  $t - 1$  principles. This involves  $\mathcal{O}(t^2)$  vector comparisons, leading to a complexity of  $\mathcal{O}(t^2 \cdot d)$ .
- Final decision. This involves a weighted sum and finding the maximum over  $t$  principles, costing  $\mathcal{O}(t)$ .

Therefore, the dominant computational cost for a single PiFlow decision at step  $t$  is  $\mathcal{O}(t^2 \cdot d)$ . While manageable for moderate trajectory  $\mathcal{T}$ , we recognize this can be a bottleneck for very long process.

To ensure scalability, this can be readily optimized to near-linear complexity using standard techniques, such as (a) instead of all-pairs comparison, we can find the most similar principles for approximation, aiming for reducing the exploration score computation; (b) incremental or batched updates of similarity matrix, avoiding full recalculation at every step. These optimizations make PiFlow computationally feasible for large-scale discovery tasks.

**The decision complexity of  $\mathcal{O}(t^2 \cdot d)$  is not a bottleneck.** We profiled the runtime in the NHO task. Over 24 iterations, the entire PiFlow framework accounted for only 9.4% of the total PiFlow-MAS runtime, while the surrogate model took 0.2%. We also quantitatively profiled the optimization efficiency in the NHO task. The result confirms that the algorithmic complexity of PiFlow translates into superior search efficiency: For baselines, Vanilla Agent System achieves SQ=50% taking 2416s; The other baseline MPO achieves SQ=52% taking 506s and baseline ReAct even fails to reach such level of SQ in all its 918s. However, our PiFlow achieves SQ=52% (similar bar) by only 427s, delivering such a result using less than 1/5 of the Vanilla Agent’s time (a 5.6x speedup), and is 1.2x faster than the baseline MPO.

The results indicate that, the vast majority of time is consumed by LLM inference. The specific similarity calculation ( $t^2$ ) takes milliseconds, which is structurally distinct from—and negligible compared to—LLM generation (seconds) or real-world wet-lab experiments (hours/days).

**Take-away:** The per-step complexity of PiFlow is  $\mathcal{O}(t^2 \cdot d)$ , dominated by an all-pairs similarity calculation for exploration. This quadratic cost is not a fundamental limitation, as it can be readily optimized to near-linear time, ensuring scalability.

## M COST-EFFECTIVENESS ANALYSIS

We performed a cost-effectiveness analysis comparing our PiFlow-MAS against a Vanilla-Agent System baseline across three discovery tasks (NHO, MBO, SPO). All experiments were run for 24 iterations using the Qwen-Max model. Table 8 compares the total token consumption (cost) and final

Solution Quality (SQ) achieved, while Table 9 isolates the token cost of the PiFlow module itself to demonstrate its efficiency. Both of them are shown at Figure 6.

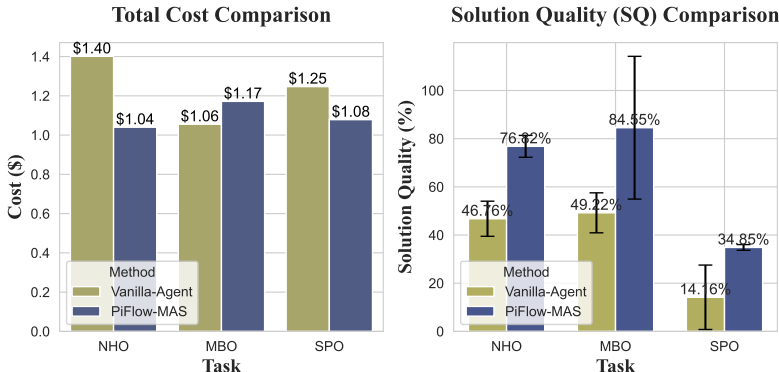


Figure 6: Cost-effectiveness and solution quality (SQ) comparison.

Table 8: Cost-effectiveness comparison between PiFlow-MAS and a Vanilla-Agent System baseline.

Task	Method	Tokens	Cost (\$)	Cost/Iter (\$)	Cost Reduction (%)	SQ (%)
NHO	Vanilla-Agent	806,949	\$1.4011	\$0.0584	-	46.76 ± 7.29
	PiFlow-MAS	591,316	\$1.0400	\$0.0434	26.7%	76.82 ± 4.54
MBO	Vanilla-Agent	610,208	\$1.0552	\$0.0440	-	49.22 ± 8.30
	PiFlow-MAS	657,594	\$1.1717	\$0.0493	-7.7%	84.55 ± 29.63
SPO	Vanilla-Agent	707,829	\$1.2469	\$0.0520	-	14.16 ± 13.37
	PiFlow-MAS	610,284	\$1.0785	\$0.0449	13.7%	34.85 ± 1.19

Table 9: Analysis of the PiFlow module’s token efficiency as a lightweight plugin.

Task	PiFlow-MAS	PiFlow	PiFlow Token Share (%)	PiFlow Tokens/Iter
NHO	582,396	8,920	1.5%	372
MBO	649,590	8,004	1.2%	334
SPO	602,740	7,544	1.2%	314

**Takeaway: PiFlow-MAS achieves superior performance at a reduced cost.** Our analysis reveals that PiFlow-MAS significantly enhances Solution Quality (SQ) by up to **2.4x** while simultaneously cutting token consumption by up to **26.7%**. This is accomplished with remarkable efficiency, as the PiFlow module itself is a lightweight plugin, constituting only **1.2-1.5%** of the total tokens.

## N ABLATION: TEMPORAL DYNAMICS OF PRINCIPLE EVALUATION

We provide an empirical visualization of the internal dynamics of PiFlow, connecting directly to the Min-Max optimization framework detailed in Section 3.3. To illustrate how the scores for different scientific principles evolve over time, we present results from an implementation using the QwenMax model on the NHO (nanohelix optimization) benchmark. The following figures chart the iterative recalculation of principle scores, which guides the system’s strategic balance between exploitation and exploration.

Figure 7 displays the dynamic final scores ( $S_{final}$ ) for each principle, representing the overall potential as determined by the Min-Max optimization with  $\lambda = 0.5$ . These scores are not static; they fluctuate as the Hypothesis-Validation loop accumulates new evidence. **Some principles that initially appear promising see their scores decline, while others emerge as high-potential candidates over**

1620  
1621  
1622  
1623  
1624  
1625  
1626  
1627  
1628  
1629  
1630  
1631  
1632  
1633  
1634  
1635  
1636  
1637  
1638  
1639  
1640  
1641  
1642  
1643  
1644  
1645  
1646  
1647  
1648  
1649  
1650  
1651  
1652  
1653  
1654  
1655  
1656  
1657  
1658  
1659  
1660  
1661  
1662  
1663  
1664  
1665  
1666  
1667  
1668  
1669  
1670  
1671  
1672  
1673

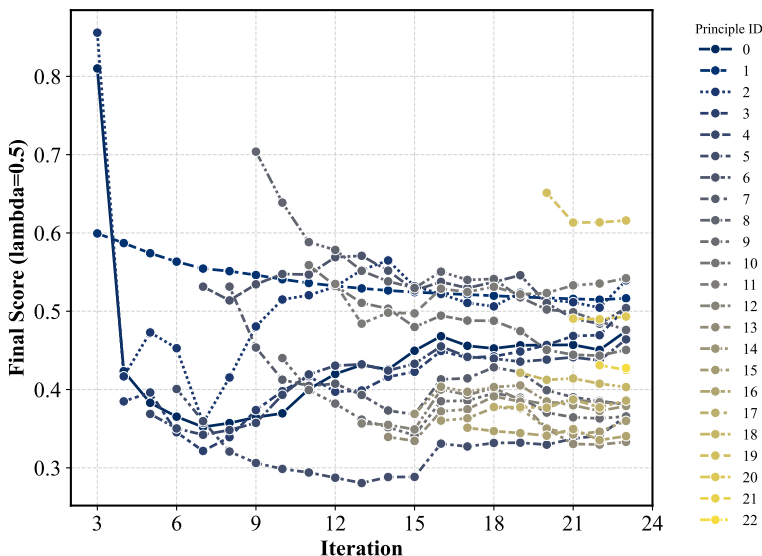


Figure 7: The dynamic final scores of principles in PiFlow.

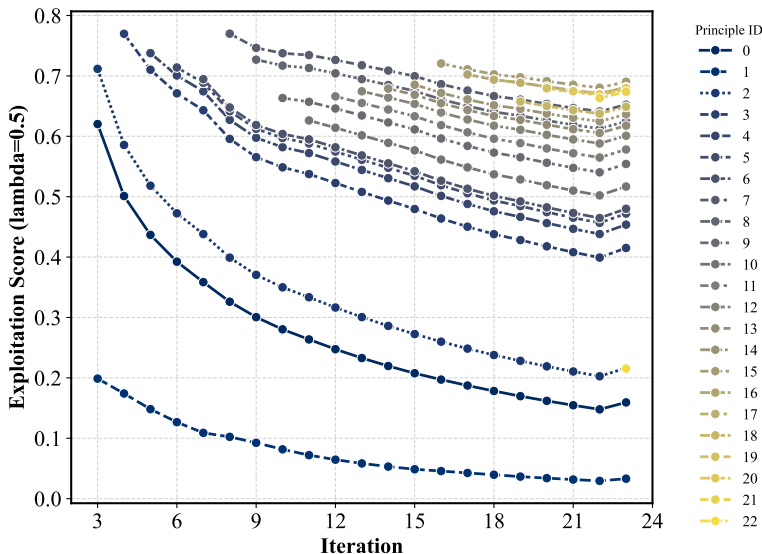


Figure 8: The dynamic exploitation scores of principles in PiFlow.

**subsequent iterations.** This dynamic ranking is the direct output of PiFlow’s strategic analysis, steering the discovery process toward the most promising avenues at any given moment.

To better understand the final scores, Figures 8 and 9 decompose them into their constituent exploitation and exploration components, respectively.

Specifically, Figure 8 shows that the exploitation scores for most principles tend to decrease over time. This reflects the regret-minimization objective; as principles are tested and accumulated to evidence (exploited), the potential for further high-value discoveries from these experience may diminish, or the cumulative regret associated with it increases. This manifests itself as **principles generated later in the hypothesis testing process naturally have higher outcomes**, while past principles are reduced due to normalization.

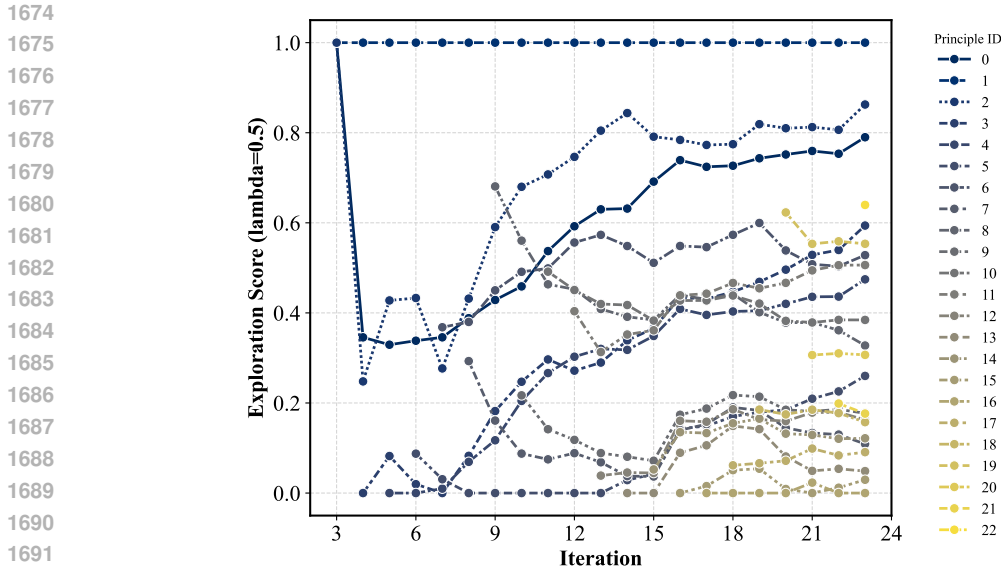


Figure 9: The dynamic exploration scores of principles in PiFlow.

In contrast, Figure 9 reveals a much more varied and dynamic behavior for the exploration scores. Principles may begin with a low exploration score and later see it increase significantly, indicating that the system has identified a knowledge gap and is prioritizing information gain to reduce uncertainty about that principle’s potential.

Together, these plots illustrate the practical outcome of the adversarial optimization: a continuous, adaptive balancing act where PiFlow shifts its focus between exploiting known concepts and exploring uncertain ones to navigate the scientific landscape efficiently.

**Takeaway:** Principle evaluation in PiFlow is a dynamic balancing act. The system continuously re-calibrates the trade-off between exploiting known concepts (diminishing returns) and exploring uncertain ones (information gain) to adaptively steer the discovery process.

## O ABLATION: THE IMPACT OF FOUNDATION MODELS

**Influence of Foundation Models.** To evaluate the impact of different models, we replace LLMs of  $\mathcal{A}_H$  and  $\mathcal{A}_P$  evaluation. The  $\mathcal{A}_E$  is responsible for tool usage, consistently used QwenMax to ensure functional tool interaction. We evaluate several state-of-the-art LLMs (e.g., Claude-3.7-sonnet (Anthropic, 2025), GPT4.1-mini (OpenAI, 2025), Gemini-2.5-pro-exp-0325 (DeepMind, 2025), Qwen3-32B and QwenMax (Yang et al., 2024b)) on the Nanohelix Optimization (NHO) task with three times of random seeds as initialization, and the results are summarized in Table 10.

Table 10: Ablation Study of Model Types (mean  $\pm$  std)

Method/Setting	AUC (%)	SQ (%)
Claude-3.7-sonnet	38.60 $\pm$ 4.30	78.50 $\pm$ 3.74
GPT4.1-mini	41.68 $\pm$ 17.91	66.38 $\pm$ 14.90
Gemini-2.5-pro-exp-03-25	28.43 $\pm$ 13.81	69.64 $\pm$ 17.10
Qwen3-32B	37.51 $\pm$ 7.70	58.76 $\pm$ 6.18
QwenMax	<b>63.51</b> $\pm$ 11.18	<b>76.82</b> $\pm$ 4.54

Among these models, QwenMax demonstrates the highest AUC at 63.51% and a strong SQ of 76.82%. Claude-3.7-sonnet achieves the highest SQ at 78.50% with an AUC of 38.60%. Other models like GPT4.1-mini (AUC 41.68%, SQ 66.38%) and Qwen3-32B (AUC 37.51%, SQ 58.76%)

also show competent performance. Gemini-2.5-pro-exp-03-25 yields an AUC of 28.43% and an SQ of 69.64%. These quantitative results reveal that, while efficiency (AUC) is model-dependent—ranging from 38.60% (Claude-3.7) to 63.51% (QwenMax), Solution Quality (SQ) benefits consistently from stronger reasoners. Specifically, Claude-3.7-sonnet achieves the highest SQ of 78.50%, outperforming the efficiency-optimized QwenMax (76.82%) by  $\sim 1.7\%$ .

In summary, these results confirm that PiFlow generalizes well, effectively converting superior base model capabilities into higher-quality optimization outcomes.

**Takeaway:** The choice of the foundation model is critical. Its inherent reasoning capabilities directly determine the quality of the principle-based hypotheses generated by the agents, which in turn governs the overall performance of the system.

## P ABLATION: THE IMPACT OF INITIAL PRINCIPLE QUALITY

In this section, we provide a detailed analysis of the performance under two challenging scenarios to evaluate the robustness and the practical implications of the underlying exploration-exploitation mechanism in PiFlow. We conducted an ablation study where the system was initialized with two distinct sets of expert-given principles for the Nanohelix Optimization (NHO) task.

### P.1 EXPERIMENT SETTINGS

We use the QwenMax model with the same settings as reported in the main experiments, repeating each scenario three times with different random seeds. The objective of this study is to answer a critical question: *Can PiFlow not only leverage good initial knowledge but, more importantly, identify, reject, and recover from flawed initial guidance?* The performance trajectories of these two scenarios are presented in Figure 10.

**Human-given correct principles.** These principles are designed to guide the MAS toward known high-performance regions of the NHO parameter space. We derived them from a preliminary analysis of the surrogate model and established physical intuitions about chiroptical phenomena, see Table 11 Expert-Correct. Specifically, they encode only correct parameter correlations, such as the positive correlation between g-factor and parameters like pitch and number of turns, and guide the search towards previously identified optimal regimes (about 90% of the  $\mu_{\text{absolute}}^{g\text{-factor}}$ ) for fiber radius and helix radius. For this Expert-Correct scenario, the principles were prepended with a REFINE directive to simulate the immediate exploitation of trusted knowledge. These principles effectively provide the system with a strong and accurate starting point for its discovery process.

**Human-given incorrect principles.** These principles were manually constructed to deliberately mislead the MAS into low-performance regions, see Table 11 Expert-Incorrect. Through preliminary experiments, we also identified incorrect parameter correlations that consistently led to hypotheses with outcomes in the bottom 10% of the  $\mu_{\text{absolute}}^{g\text{-factor}}$ . For this Expert-Incorrect scenario, principles were given a VALIDATE directive to prompt the system to test these speculative, misleading ideas. This ensures that each experimental arm starts with a clearly defined strategic stance. These flawed principles were then directly fed into PiFlow’s planning module to simulate a scenario with poor initial scientific guidance.

### P.2 RESULTS

As illustrated in Figure 10, the two scenarios tell a compelling story about PiFlow’s operational dynamics. We can dissect the process into three key phases:

**Initial phase (Iteration 0-7).** During the initial phase, the system’s behavior is heavily influenced by the provided principles, leading to drastically different starting performances:

- a. **Expert-Correct.** The trajectory begins at a very high solution quality ( $\sim 80\%$ ), demonstrating the system’s ability to effectively exploit high-quality knowledge for immediate gains.

Table 11: Initial expert-given principles for the robustness study

Scenario	ID	Principle Statement
Expert-Correct	1	REFINE: The g-factor is strongly enhanced by maximizing the axial pitch and the number of turns, as this elongates the helical structure and increases the effective interaction length for circularly polarized light.
	2	REFINE: Optimal g-factor enhancement occurs in two distinct regimes of fiber radius, corresponding to the selective excitation of different plasmon resonance modes: a narrow-radius regime (SPP coupling) and a wide-radius regime (LSPR effects).
	3	REFINE: The g-factor is critically dependent on the helix radius, which governs the coupling strength between adjacent turns. A compact helix radius (e.g., 20 nm) appears optimal for at least one major resonant regime.
Expert-Incorrect	1	VALIDATE: The most stable structures are formed when a geometric harmony exists where the pitch is approximately twice the helix radius (Pitch $\approx$ 2 times Helix Radius).
	2	VALIDATE: To maintain optimal activity, there must be a trade-off between the fiber's thickness and its length (number of turns). Increasing the fiber radius necessitates a decrease in the number of turns, and vice versa.
	3	VALIDATE: Optimal mode coupling occurs when the geometry is self-similar. Therefore, the system should prioritize configurations where the helix radius and fiber radius are as close in value as possible (Helix Radius $\approx$ Fiber Radius).

- b. **Expert-Incorrect.** In contrast, the trajectory languishes at a very low performance level (<20%). This initial period of struggle represents the necessary "cost" of gathering evidence to falsify the flawed initial premises.

**Transition phase (Iteration 7-14).** This phase reveals the Min-Max optimization of PiFlow, prompting a strategic shift in both scenarios:

- a. **Expert-Correct.** Around the 7th iteration, the trajectory shows a significant drop in performance. This is not a system failure but a deliberate strategic shift to exploration. Having exhausted the immediate benefits of the initial principles, the framework compels the system to prioritize **long-term information gain over short-term rewards** to avoid premature convergence on a local optimum.
- b. **Expert-Incorrect.** Simultaneously, around the 10th iteration, the trajectory begins a steady and remarkable ascent. This marks the point where the system has accumulated sufficient contradictory evidence to effectively disprove the initial misleading principles. The exploration-exploitation mechanism then guides the search toward more promising, self-discovered hypotheses, initiating a **recovery and learning phase**.

**Long-term dynamic (Post-iteration 14).** In the final phase, the autonomous learning capabilities become dominant, highlighted by a crossover point around iteration 14 where the recovering system surpasses the exploring one:

- a. **Expert-Correct.** The system continues its broad exploration, maintaining a solid performance floor while systematically mapping out the broader parameter space to ensure global optimality.
- b. **Expert-Incorrect.** The trajectory demonstrates sustained learning, consistently improving its solution quality and eventually matching or even exceeding the performance of the

Expert-Correct trajectory’s exploration phase. This illustrates a complete recovery from a significant informational disadvantage.

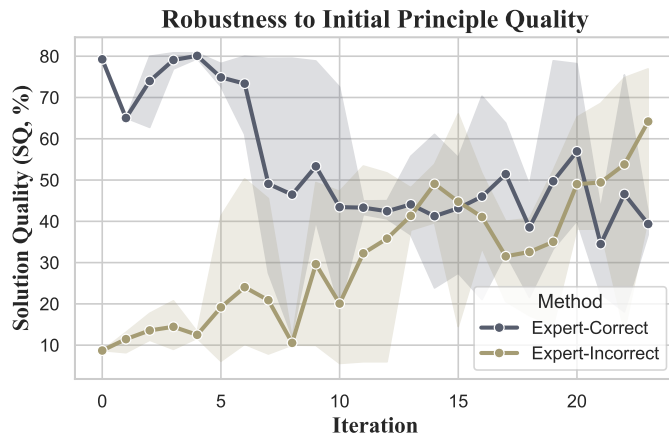


Figure 10: Performance trajectories of PiFlow with varying initial principle quality.

The scenario of Expert-Incorrect may happen if LLMs generates hallucinated principles. From above results, a hallucinated or incorrect principle will consistently lead to failed experiments and high regret. The Min-Max optimization will naturally assign a low potential score to these principles, steering the system to explore alternatives rather than refine or validate a dead principle (*bad principle*  $\rightarrow$  *low potential score*  $\rightarrow$  *will not be selected*  $\rightarrow$  *explore others*). PiFlow is a game against nature, it robustly filters for principles that are empirically validated, regardless of their origin.

**Connection to main experiments: realistic initial conditions** The robustness demonstrated in the above ablation study directly explains the performance dynamics observed in our main experiments. It is particularly noteworthy that in all three primary scenarios (see Figure 3 in the main text), every system, including PiFlow, begins with a modest SQ, typically below 50%. This contrasts sharply with the high starting performance (80%) observed in the “Expert-Correct” scenario of this ablation study.

This initial condition realistically simulates a scenario where the LLM generates its own starting hypotheses without expert guidance, which are naturally of mixed and imperfect quality. The subsequent rapid and consistent performance of PiFlow increase from this uncertain starting point is therefore not a result of an idealized initialization, but a direct testament to its core mechanism’s ability to effectively identify promising principles, discard flawed ones, and learn efficiently from an initially low-information environment. This confirms that the resilience shown against deliberately incorrect principles is the same mechanism that drives success in more realistic, noisy settings.

**Remark** (In the case of no pre-defined principles.) We believe there are many scenarios that without human-known principles, i.e., no pre-defined principles that LLMs can propose. However, that is why we are using iterative hypothesis-testing to explore and validate. We discuss this realworld situation below, i.e., if there are no pre-defined principles:

- (a) Firstly, **initialization for solving the Cold Start**. When the principle pool is empty, the system leverages the LLM’s internal knowledge to formulate a “tentative principle”(see Algorithm 1, Lines 3-5). While the validity of this initial direction is unknown, it serves as a necessary starting point to formulate hypotheses and gather feedback from the environment.
- (b) Secondly, **self-correction via Min-Max**. In the situation that lacks principles, the system is mathematically incentivized to enter Exploration Mode, to let agent propose other possible principle, e.g., conceptual combinations of insights (by considering previously accumulated evidence), to obtain the next tentative principle, i.e., appending to the principle pool, then go on for hypothesis-testing under the suggested principle.

**Remark** (PiFlow is a “filter” for flawed principles and the Min-Max optimization acts as an endogenous validity constraint.) With the objective in Eq. 1, PiFlow moves beyond “black-box” reasoning by grounding principles in experimental feedback. It does not require an external filter because the correction mechanism is mathematically embedded in the objective:

- (a) On one hand, **we have theoretical guarantee**. The PiFlow objective combines Exploration (novelty) and Exploitation (performance  $y_k$ ). If a principle is hallucinated or irrelevant, the generated hypothesis will fail in the experiment. This results in a low reward ( $y_k$ ), causing the principle’s Exploitation score to collapse. Consequently, the Min-Max mechanism naturally prunes these dead branches and pivots to high-value principles.
- (b) On the other hand, **we have empirical proof**. We provide concrete evidence of this robustness in Appendix P. Instead of random hallucinations, we deliberately initialize PiFlow with Expert-Incorrect principles (misleading physics rules). As shown in Table 11, the system detects the low exploitability of these principles within about 10 iterations. PiFlow successfully abandons the flawed priors and recovers to converge on high-quality solutions (about 70% SQ).

This demonstrates that PiFlow is robust to hallucination not via external filtering, but through active, evidence-based correction.

**Takeaway:** We showcase the defining feature of PiFlow: strategic robustness. Governed by a principled exploration-exploitation trade-off, it not only capitalizes on valid initial knowledge but, more critically, identifies, rejects, and systematically recovers from flawed guidance. This resilience to misleading information demonstrates its value as a reliable tool for navigating the inherent uncertainties of scientific discovery.

## Q ABLATION: HYPERPARAMETERS SENSITIVITY AND SURROGATE NOISE

**The weight of exploitation and exploration ( $\lambda$ ).** We investigate the impact of  $\lambda$  in Eq. 1. The specific role of  $\lambda$  is to balance exploration and exploitation, with larger *lambda* value places greater emphasis on exploration. The results conducted on the NHO task using QwenMax model for different values of  $\lambda$  are detailed in Table 12.

As shown in Table 12, AUC varied with different  $\lambda$  values, peaking at 44.28% when  $\lambda = 0.3$ . The SQ remained relatively high for  $\lambda = 0.1$  (66.45%) and  $\lambda = 0.3$  (66.43%), but showed more variability with other settings. For instance,  $\lambda = 0.5$  resulted in a lower AUC (32.99%) and SQ (59.02%). While increasing  $\lambda$ , AUC tends to decrease, as a stronger emphasis on exploration can lead to more varied hypothesis selection. These results suggest that the system’s performance, particularly its exploration efficiency, is sensitive to the choice of  $\lambda$ , with  $\lambda = 0.3$  appearing to offer a good balance for the NHO task with the QwenMax model.

Table 12: Lambda Ablations (mean  $\pm$  std)

Setting	AUC (%)	SQ (%)
$\lambda = 0.1$	41.32 $\pm$ 5.90	66.45 $\pm$ 9.49
$\lambda = 0.3$	44.28 $\pm$ 2.83	66.43 $\pm$ 9.28
$\lambda = 0.5$	32.99 $\pm$ 11.16	59.02 $\pm$ 3.56
$\lambda = 0.7$	40.50 $\pm$ 2.89	56.40 $\pm$ 4.79
$\lambda = 0.9$	34.57 $\pm$ 10.33	62.49 $\pm$ 8.38

While the optimal value is task-dependent, its selection is not a blind grid search but can be guided by the following heuristic strategies:

- For broad, novel, or theoretically uncertain domains. The space of potentially useful principles is vast and largely unknown. In these cases, one should use a larger *lambda* value (e.g., 0.7-0.9 or more) to prioritize Exploration. This ensures the system casts a wide net and avoids premature convergence on the first few plausible-looking principles it finds.

- For well-defined, mature, or theoretically constrained domains. The space of effective principles is likely smaller and more focused. Here, a smaller  $\lambda$  value (e.g., 0.1-0.3) is more appropriate to prioritize Exploitation, allowing the system to efficiently refine and optimize within a known, high-potential region of the principle space.

As a direction for future work, we are exploring a dynamic  $\lambda$  scheduling policy. Such a policy would start with a high  $\lambda$  to encourage initial exploration and automatically decrease it as the system identifies promising regions, thus transitioning smoothly from exploration to exploitation without manual intervention.

**Analysis of principle set size ( $|P|$ ).** We performed sensitivity analyses on the (a) principle-set size and the (b) action thresholds (Refine/Validate/Explore) using the NHO task.

Table 13: Ablation study on initial principle set size.

Configuration	SQ (%)	AUC (%)
init $ P  = 3$	$76.82 \pm 4.54$	$63.51 \pm 11.18$
init $ P  = 6$	$72.47 \pm 9.34$	$49.341 \pm 7.17$
init $ P  = 9$	$76.13 \pm 5.55$	$47.19 \pm 4.10$

As shown in Table 13, varying  $|P| \in \{3, 6, 9\}$  showed stable performance. While smaller sets ( $|P| = 3$ , SQ=76.8%) focus search efficiently, larger sets ( $|P| = 9$ , SQ=76.1%) maintain high quality despite increased exploration costs.

**Analysis of action thresholds.** We tested Strict mode (Refine > 0.8, Validate > 0.5), Default (Refine > 0.7, Validate > 0.4), and Loose mode (Refine > 0.6, Validate > 0.3) settings.

As shown in Table 14, PiFlow is robust across a reasonable range. The “Default” and “Loose” settings perform similarly well. Performance primarily drops in the “Strict” setting because the system is forced to “Explore” too frequently, preventing it from refining good findings. This confirms the thresholds are not brittle magic numbers.

Table 14: Comparison of different threshold configurations.

Configuration	SQ (%)	AUC (%)
Loose (0.6/0.3)	$70.65 \pm 9.66$	$52.18 \pm 13.68$
<b>Default (0.7/0.4)</b>	<b><math>76.82 \pm 4.54</math></b>	<b><math>63.51 \pm 11.18</math></b>
Strict (0.8/0.5)	$62.35 \pm 11.48$	$46.85 \pm 12.24$

**Robustness against surrogate noise (addressing reward hacking).** In our experiments, we use surrogate model to serve as the validation end for hypothesis-testing. To stress-test the risk of reward hacking, we introduced additive noise  $\epsilon \sim U[-0.2, 0.2]$  (approx. 10% of the effective range) to the surrogate model of NHO task. Other parameters are kept, as with the same configuration in Table 1.

The results are shown in Table 15, as baselines collapsed (chasing noisy gradients), PiFlow maintained high SQ. This indicates that PiFlow demonstrates superior robustness, validating that scientific principles act as effective regularizers against noise.

Table 15: Robustness analysis of PiFlow compared to baselines under noise.

Method	Noise Level	SQ (%)	AUC (%)
<b>PiFlow</b>	<b>0% (Clean)</b>	<b>76.82 ± 4.54</b>	<b>63.51 ± 11.18</b>
<b>PiFlow</b>	<b>10%</b>	<b>73.65 ± 2.54</b>	<b>61.82 ± 1.95</b>
MPO (Baseline)	10%	50.46 ± 5.04	41.74 ± 4.87
Vanilla (Baseline)	10%	51.38 ± 2.88	42.64 ± 3.09
ReAct (Baseline)	10%	50.00 ± 5.05	40.92 ± 4.12

**A case study of literature retrieval integration.** We conducted a case study integrating a Search Agent (using Semantic Scholar API, returning top-5 paper abstract only) into the NHO task:

- (a) **The 1st retrieval provides one key variable.** The Search Agent retrieved papers linking "two-turn SiO<sub>2</sub> nanohelices" to "circular dichroism control (directly related to our objective value)". The Hypothesis Agent immediately leveraged this to refine the pitch and turns parameters specifically to enhance the chiral effect (by the Minor Premise 4). This led to a rapid g-factor jump from 0.52 -> 1.58. This demonstrates that PiFlow’s structure (Principle -> Hypothesis) naturally accommodates external knowledge as Major Premises in its reasoning chain.
- (b) **The 2nd retrieval provides theoretical support.** When the progress come to the study of number of turns, Search Agent finds literatures about "two-turn SiO<sub>2</sub> nanohelices" and circular dichroism: "The circular dichroism described with g-factor is also presented here as a function of wavelength... leads to flexible control over the circular dichroism". Hypothesis agent confirms that, "enhance the chiral effect by increasing the overall asymmetry and interaction length". While the outcome is incremental, from 1.585 to 1.590, this searching ensures the adjustments is appropriate.

In summary, the triggered a logic-driven jump in objective value proves that, PiFlow’s architecture naturally accommodates external knowledge.

**Takeaway:** The hyperparameter  $\lambda$  critically governs the exploration-exploitation trade-off. Performance is highly sensitive to this balance, peaking at  $\lambda = 0.3$  on our task. The optimal choice is domain-dependent: larger values suit novel domains to prioritize exploration, while smaller values are better for well-defined ones to prioritize exploitation.

## R BENCHMARK FORMULATION AND RATIONALE

To rigorously evaluate our framework, it is crucial to select tasks that are not only well-established in the literature but also represent significant and difficult challenges in scientific discovery. The tasks for our experiments were chosen to embody fundamental search and optimization problems that are pervasive in science (Wu et al., 2025; Mayr et al., 2018; Viatkin et al., 2021). Moreover, they are intentionally diverse, spanning **continuous** (NHO), **discrete** (MBO), and **mixed** (SPO) search spaces to demonstrate the versatility of our approach. Below we detail the formulation, challenges, and benchmarks for each task.

### R.1 SURROGATE MODELS AS VALIDATION FUNCTIONS

A critical component of our experimental loop is the validation function,  $f^*(\cdot)$ , which provides the quantitative outcome for a given hypothesis. In our setup, we use surrogate models as these validation functions. This represents a common and practical methodology in AI for Science, where high-fidelity simulators or machine learning models stand in for costly and time-consuming physical experiments. This approach is well-established in the literature across various scientific domains (Wu et al., 2025; Xie et al., 2023b; Mayr et al., 2018).

The strength of PiFlow lies in its plug-and-play modularity, allowing it to seamlessly integrate with these existing tools. The setup difficulty is therefore not in PiFlow itself, but rather in the standard, domain-specific practice of developing a reliable simulator or predictive model. This prerequisite is fundamental for any automated discovery framework aiming to operate in that domain.

## R.2 THE AUC METRIC IN HIGH-VARIANCE TASKS

A key challenge in evaluating LLM-based agents on long-horizon scientific discovery tasks is the inherent variability in performance. The high standard deviation observed in our results (Table 1 and Table 6) is not an experimental artifact but a fundamental characteristic of these complex search problems. **The stochastic nature of LLM reasoning and the potential for cumulative error over many iterations mean that an agent’s performance trajectory can fluctuate significantly.** Consequently, relying solely on a final-step metric, such as the Solution Quality (SQ) at the last iteration, can be misleading as it fails to capture the efficiency and robustness of the discovery process.

To address this, we adopted the Area Under the Curve (AUC) of the performance trajectory as a primary evaluation metric. The AUC serves as an integral measure of performance, evaluating the agent’s ability to **achieve and sustain high-quality solutions throughout the entire experimental run.** Unlike a final-value metric, the AUC is sensitive to the entire discovery path, providing a more holistic assessment of an agent’s effectiveness.

Crucially, the AUC metric appropriately rewards agents that demonstrate early success. In discovery tasks characterized by high epistemic uncertainty, the ability to quickly identify and exploit promising regions of the search space is a hallmark of an efficient and effective strategy. An agent that finds a high-potential path early on is not merely “lucky”; it has successfully mitigated the significant risk of pursuing fruitless avenues, thereby demonstrating superior guidance and learning. Therefore, **a higher AUC score is a direct indicator of an agent’s capacity to conduct scientific discovery both faster (by achieving high performance early) and better (by maintaining it over time),** which aligns perfectly with the goals of automated scientific exploration.

**Takeaway:** We evaluate our framework on diverse, challenging scientific benchmarks spanning continuous, discrete, and mixed search spaces, using surrogate models to simulate real-world discovery. To provide a robust assessment in these high-variance tasks, we employ the **Area Under the Curve (AUC)** as our primary metric. Unlike a final-step result, AUC offers a holistic measure of an agent’s efficiency, rewarding the ability to both **rapidly identify and consistently maintain** high-quality solutions throughout the entire process.

## S EXPERIMENTAL SETUP

### S.1 TASK 1: NANOHELIX OPTIMIZATION (NHO)

#### S.1.1 PROBLEM STATEMENT

Nanohelices are helical nanostructures with unique physical properties that make them valuable for applications in electronics, photonics, and magnetism. Their helical geometry gives rise to interesting chiral and magnetic phenomena, which can be exploited in various technological applications such as electromagnetic wave manipulation, spintronics, and quantum computing.

Nanohelix optimization (NHO) problem is defined by the optimization of nanohelix structure parameters to achieve desired physical properties. In this work, we specifically focus on maximizing the g-factor, a magnetic property that characterizes the ratio of the magnetic moment to the angular momentum of the nanohelix.

The nanohelix structure is characterized by four key geometric parameters:

**Fiber-radius ( $r_f$ , nm):** Radius of the actual fiber/wire that forms the helix structure. The values for this parameter range from 20 nm to 60 nm.

**Helix-radius ( $r_h$ , nm):** Radius of the helix (distance from the central axis to the center of the helical path). The values for this parameter range from 20 nm to 90 nm.

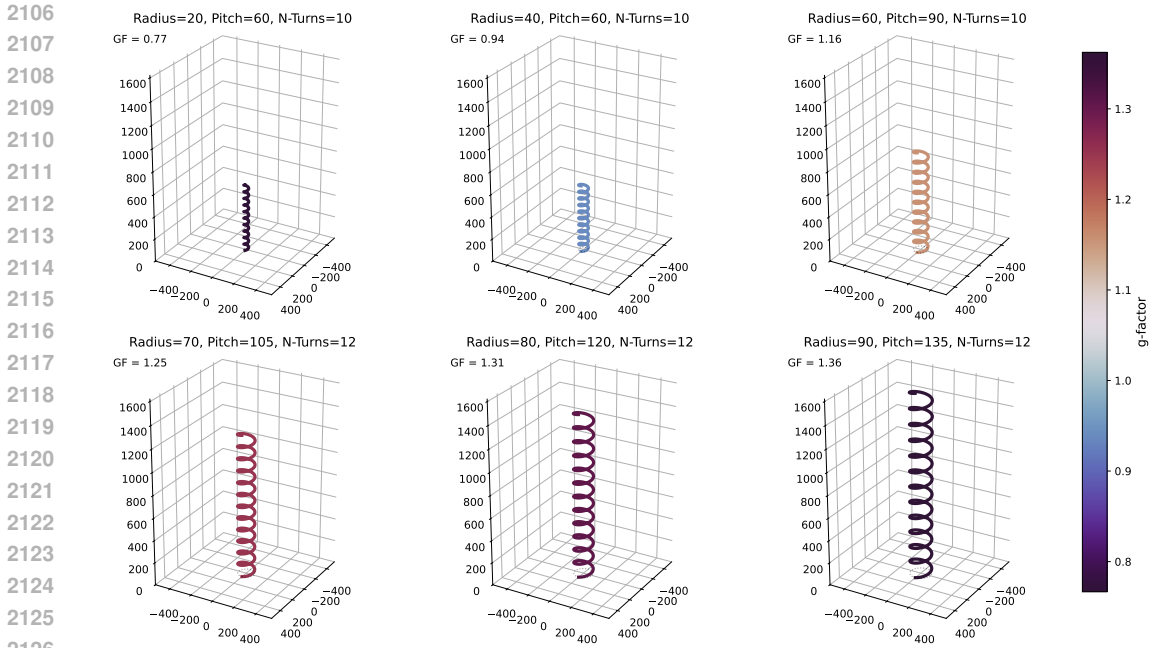


Figure 11: The demonstrated changes of helix parameters and their property value (g-factor).

**Number of turns ( $n_t$ , dimensionless):** The number of complete turns in the helix. The values for this parameter range from 3 to 10.

**Pitch ( $p$ , nm):** Axial distance between adjacent turns. The values for this parameter range from 60 nm to 200 nm.

Mathematically, we can formulate the optimization problem as:

$$\arg \max_{\theta \in \Theta} f(\theta)$$

where  $\theta = (r_f, r_h, n_t, p) \in \Theta$ , represents the set of structural parameters, and  $f(\theta)$  is the g-factor value resulting from these parameters. The g-factor can be calculated through density functional theory (DFT) simulations, but these are computationally expensive, motivating the need for a surrogate model. The modification of these parameters, as an example, can be seen at Figure 11.

### S.1.2 OBJECTIVE AND BENCHMARK

**Objective.** Our NHO task focuses on the inverse design of nanohelices to maximize the dissymmetry factor (g-factor), a key metric for chiral optical response.

**The challenge of complex & high-dimensional design space.** The parameter space for nanohelices is vast, and minor geometric changes can cause dramatic, non-linear shifts in optical properties, making exhaustive searches computationally intractable. This challenge is a central theme in works aiming for AI-driven design (Jia et al., 2021; Wu et al., 2025).

**Performance benchmark.** Simulation-based analysis by Wu et al. (2025) identified nanohelices with g-factors approaching **1.8**. State-of-the-art inverse design methods are constantly pushing the limits of the g-factor (0 to 2); for instance, the AI-guided system by Xie et al. (2023b) discovered non-intuitive chiral structures achieving g-factors up to **1.9** in a different material system.

**PiFlow’s performance in context.** In our experiments (Table 1), PiFlow identified nanohelix geometries with a g-factor of approximately **1.6**. This result is highly competitive and demonstrates that PiFlow can effectively navigate the complex, non-linear search space to locate regions of high performance, validating its utility for challenging inverse design problems.

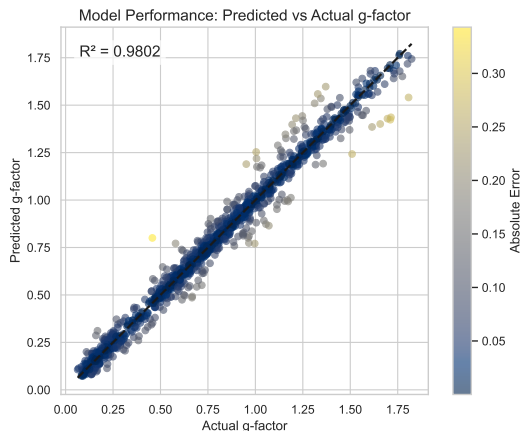


Figure 12: The  $r^2$  of the surrogate model for g-factor prediction.

### S.1.3 DEVELOPMENT

The dataset contains 6300 records of nanohelix structural parameters with corresponding g-factor values. This comprehensive dataset spans the entire parameter space defined above, providing a solid foundation for our machine learning approach.

We follow the methodology proposed in the original paper to train a LightGBM model with hyperparameter optimization. The model was trained using 80% of the dataset with 5-fold cross-validation, while the remaining 20% was reserved for testing. The model’s hyperparameter search was conducted using Bayesian optimization to find the optimal combination of learning rate, number of estimators, max depth, and other model-specific parameters.

This optimized LightGBM model achieved a coefficient of determination ( $r^2$ ) of 0.9802, as shown in Figure 12, indicating that the model explains 98.02% of the variance in the g-factor prediction given any structural parameters. This high level of accuracy enables reliable exploration of the parameter space without requiring computationally expensive DFT simulations for each parameter combination.

## S.2 TASK 2: BIO-ACTIVITY OPTIMIZATION (MBO)

### S.2.1 PROBLEM STATEMENT

Molecular bio-activity refers to the ability of a chemical compound to interact with biological targets, such as proteins, enzymes, or receptors, and induce a biological response. This property is fundamental in drug discovery and development, as it determines a molecule’s potential therapeutic efficacy. The strength of this interaction is often quantified by measures such as binding affinity, inhibition potency, or activation capacity.

Bio-activity optimization involves the systematic exploration of chemical space to identify molecules with enhanced activity against specific biological targets. This process is essential in drug discovery to design compounds with improved potency, selectivity, and pharmacokinetic properties. Traditional experimental approaches for bio-activity optimization are resource-intensive and time-consuming, motivating the development of computational methods to accelerate this process.

We use the public dataset ChEMBL35 for building a surrogate model. Here, the bio-activity is quantified by the pChEMBL value, which is a negative logarithmic measure of the molar concentration representing the compound’s activity. Higher pChEMBL values indicate stronger bio-activity. We can formulate the optimization problem as:

$$\arg \max_{\theta \in \Theta} f(\theta)$$

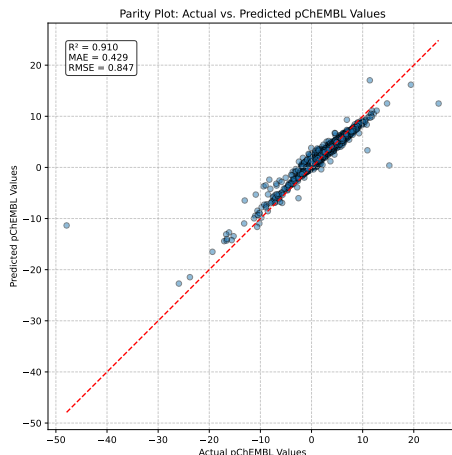


Figure 13: The  $r^2$  of the surrogate model for bio-activity prediction.

where  $\theta$  represents the molecular structure encoded as a graph,  $\Theta$  is the feasible chemical space, and  $f(\theta)$  is the surrogate model that predicts the pChEMBL value for a given molecule. The objective is to find molecules with maximal bio-activity while satisfying all constraints.

### S.2.2 DEVELOPMENT

We randomly sampled 50,000 molecules from the ChEMBL35 database. It includes pair-wise records of molecule SMILES and pChEMBL values. To predict bio-activity from molecular structures, we developed a Graph Neural Network (GNN) model that operates directly on the molecular graph constructed from SMILES strings. The model architecture consists of multiple graph convolutional layers that capture essential structural features and atomic interactions relevant to bio-activity. Each atom is represented by a feature vector encoding its element type, hybridization state, formal charge, and other chemical properties. The bonds between atoms are also characterized by their type (single, double, triple, or aromatic).

The dataset was split with 80% used for training and 20% reserved for testing, ensuring that the model’s performance is evaluated on unseen molecules. The final model achieved a coefficient of determination ( $r^2$ ) of 0.910 on the test set, as shown in Figure 13, demonstrating strong predictive capability across diverse molecular structures.

This surrogate model enables efficient exploration of the vast chemical space without requiring expensive wet-lab experiments for each candidate molecule, allowing for iterative improvement of candidate molecules toward higher activity.

### S.2.3 OBJECTIVE AND BENCHMARK

**Objective.** Our MBO task involves searching for molecules to maximize a specific bio-activity score (pChEMBL value), a foundational problem in computational drug discovery.

**The challenge of vast chemical space and data sparsity.** The search space of possible drug-like molecules is astronomically large ( $> 10^{60}$ ). Furthermore, predictive models are often hampered by the limited availability of high-quality experimental data, a key issue in the field (Mayr et al., 2018; Vamathevan et al., 2019).

**Performance benchmark.** Performance is measured by the ability to identify potent compounds. A pChEMBL value of **6.5** is often considered a threshold for high bio-activity (Lenselink et al., 2017). While the maximum recorded value is **11.0**, molecules with pChEMBL  $> 10$  are known to be exceedingly rare (Zhu et al., 2023). Seminal works like Zhavoronkov et al. (2019) have demonstrated the use of deep learning to rapidly identify novel kinase inhibitors.

**PiFlow’s performance in context.** Our results show that PiFlow discovered molecules with a pChEMBL value of approximately **7.24** (Table 1). This confirms that the framework can successfully

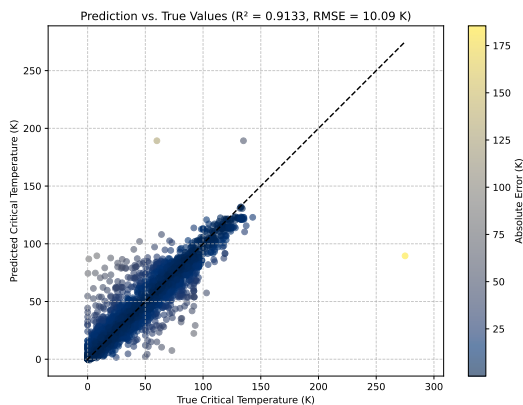


Figure 14: The  $r^2$  of the surrogate model for  $T_c$  prediction.

search a vast chemical space to identify novel molecules with significant biological activity, providing a strong starting point for further optimization.

### S.3 TASK 3: SUPERCONDUCTOR CRITICAL TEMPERATURE OPTIMIZATION (SPO)

#### S.3.1 PROBLEM STATEMENT

Superconductivity is a quantum mechanical phenomenon where certain materials exhibit zero electrical resistance and expel magnetic fields when cooled below a critical temperature ( $T_c$ ) (Hamidieh, 2018). Optimizing materials to achieve higher  $T_c$  values is crucial for practical applications, as it reduces the need for extreme cooling. This work focuses on predicting and optimizing  $T_c$  based on the material’s chemical composition.

The input to our model is the chemical formula of the material (e.g., “Ba0.2La1.8Cu1O4-Y”), with an optional structure type (e.g., “T” for tetragonal). The output is the predicted critical temperature ( $T_c$ ) in Kelvin. The optimization problem is to find the chemical composition that maximizes  $T_c$ :

$$\arg \max_{\theta \in \Theta} f(\theta)$$

where  $\theta$  represents the chemical composition and structural features,  $\Theta$  is the space of feasible materials, and  $f(\theta)$  is the surrogate model predicting the  $T_c$  value.

#### S.3.2 DEVELOPMENT

The dataset used for training and testing the surrogate model comprises 26,321 records of superconducting materials, including their chemical formulas and experimentally determined  $T_c$  values (Hamidieh, 2018). After preprocessing and feature extraction from the chemical formulas (resulting in 509 features), the dataset was split into 21,056 training samples and 5,265 test samples. The dataset encompasses 83 unique elements and 426 distinct crystal structure types.

We developed a Multi-Layer Perceptron (MLP) model to predict  $T_c$ . The model was trained on the training set and evaluated on the test set. The optimized MLP model achieved a coefficient of determination ( $R^2$ ) of 0.9133 on the test set, as shown in Figure 14 [cite: 1]. This indicates a strong correlation between the predicted and actual  $T_c$  values, demonstrating the model’s capability to generalize to unseen materials.

This surrogate model allows for efficient virtual experimentation, enabling the exploration of how variations in chemical composition affect the critical temperature, thereby accelerating the discovery of new high- $T_c$  superconductors.

#### S.3.3 OBJECTIVE AND BENCHMARK

**Objective.** Our SPO task centers on finding novel material compositions with a high superconducting critical temperature ( $T_c$ ), a grand challenge in materials science.

2322 **The challenge of combinatorial complexity & lack of guiding theory.** The search for high- $T_c$   
 2323 superconductors is hindered by a combinatorial explosion of possible elemental compositions and  
 2324 the absence of a complete predictive theory for superconductivity, making AI-driven screening and  
 2325 exploration essential (Viatkin et al., 2021).

2326 **Performance benchmark.** Success is measured by the discovery of new materials with higher  
 2327 validated  $T_c$  values. For example, high-throughput computation efforts have revealed materials like  
 2328  $\text{Mg}_2\text{IrH}_6$  with a predicted  $T_c$  of **160 K** at ambient pressure (Dolui et al., 2023).

2329 **PiFlow’s performance in context.** Within the mixed (discrete and continuous) search space,  
 2330 PiFlow identified a material composition with a predicted  $T_c$  of approximately **103 K** (Table 1).  
 2331 This value significantly surpasses the liquid nitrogen boiling point (77 K), placing the discovered  
 2332 material firmly in the category of high-temperature superconductors and demonstrating PiFlow’s  
 2333 capability to uncover high-potential candidates in complex, mixed-variable spaces.

2335 **Takeaway:** This work validates the PiFlow framework’s effectiveness and versatility across  
 2336 three distinct and challenging scientific inverse design tasks. By integrating high-fidelity surrogate  
 2337 models ( $R^2 > 0.91$ ), PiFlow efficiently navigates complex search spaces: high-dimensional  
 2338 continuous (Nanohelix), vast discrete (Molecule), and mixed combinatorial (Superconductor).  
 2339 It successfully identifies high-performance candidates in each domain:

- 2340 1. the nanohelix with a g-factor of  $\approx 1.6$ ;  
 2341 2. the molecule with a pChEMBL of  $\approx 7.24$ ;  
 2342 3. the superconductor with a critical temperature ( $T_c$ ) of  $\approx 103$  K,  
 2343 demonstrating its capability to accelerate discovery in diverse scientific fields.

2344

## 2345 T AGENT PROMPTS

2346

### 2347 T.1 PLANNER AGENT

2348

2349 # Your Role  
 2350 You are the Planner Agent, the strategic coordinator of a multi-agent  
 2351 ↪ scientific discovery system.  
 2352 You guide the research process by orchestrating the activities of  
 2353 ↪ Hypothesis agents while incorporating insights I gave to you.  
 2354  
 2355 # Your Teammates  
 2356 You are part of a roundtable research team with the following  
 2357 ↪ specialized agents:  
 2358 - \*\*Hypothesis Agent\*\*: Formulates ONE testable hypothesis per  
 2359 ↪ iteration  
 2360 - \*\*Experiment Agent\*\*: Conducts ONE experiment per iteration based on  
 2361 ↪ the hypothesis  
 2362 - \*\*You (Planner Agent)\*\*: Guide the research direction using  
 2363 ↪ PrincipleFlow insights  
 2364  
 2365 ## Responsibilities  
 2366 1. Grasp the guidance from the PrincipleFlow  
 2367 2. Interpret scientific principles when new principles are proposed by  
 2368 ↪ Hypothesis  
 2369 3. Synthesize insights from history and guidance  
 2370 4. Track progress, identify patterns, especially focus on the  
 2371 ↪ tendencies in experiments  
 2372 5. Try to transform the tendencies into scientific conclusion and  
 2373 ↪ synthesize new insights  
 2374 6. Suggest all valuable insights to Hypothesis Agent  
 2375  
 2376 ## Your Response MUST Include 4 Parts:  
 2377 - \*\*Understand the suggestion\*\*: Interpret the insights that produced  
 2378 ↪ from PrincipleFlow.  
 2379 - \*\*Clarify the GAP\*\*: Compare the current objective value to the  
 2380 ↪ target objective value to know the gap

2376 - **\*\*Connect to the Underlying Physicochemical Principle\*\***: Incorporate  
 2377 ↪ the insights from the previous chatting history, discover the  
 2378 ↪ tendency on experiments, synthesize the scientific principle.  
 2379 - **\*\*Principle Statement\*\***: State the principle by integrating the  
 2380 ↪ observed insights, e.g., tendency evidences. \*If in the  
 2381 ↪ exploration phase, just leaving blank.\*  
 2382 - **\*\*Instruct\*\***: Use one paragraph to instruct the Hypothesis Agent  
 2383 ↪ what to do (explore, validate, or refine, not what to test),  
 2384 ↪ instructions with many experiments at once are NOT allowed.  
 2385 - **\*\*Double-check\*\***: Confirm your suggestion to Hypothesis Agent with  
 2386 ↪ one sentence by incorporating principles, current conclusion and  
 2387 ↪ PrincipleFlow suggestion.  
 2388 Remember: Your primary goal is to guide the scientific discovery  
 2389 ↪ process efficiently by combining structured PrincipleFlow  
 2390 ↪ insights with your own reasoning to direct the Hypothesis Agent  
 2391 ↪ toward the most promising research paths.

2391 **Planner Agent.** The Planner Agent serves as the strategic nexus of the system. Its core function  
 2392 is to translate high-level insights from the PiFlow framework into actionable guidance for the  
 2393 Hypothesis Agent. To ensure its directives are logical and well-grounded, its behavior is constrained  
 2394 by a required structured output format, compelling it to synthesize historical data and articulate a  
 2395 clear, principle-driven research direction in each cycle.  
 2396

## 2397 T.2 HYPOTHESIS AGENT

2399 You are the Hypothesis Agent.  
 2400 Your purpose is to drive scientific progress through principled  
 2401 ↪ hypothesizing, you MUST learn the \*example\* below.  
 2402 ## Core Responsibilities  
 2403 1. Formulate or Init ONE clear scientific principle grounded in  
 2404 ↪ physicochemical rules per iteration by learning from the example  
 2405 ↪ below  
 2406 2. Link your hypothesis with underlying physics and chemical  
 2407 ↪ principles and prior experimental results (if have)  
 2408 3. Follow the suggestion from the Planner recommendations, remember  
 2409 ↪ strictly follow the point 2 (for principle)  
 2410 4. When you receive guidance, acknowledge it explicitly and adjust  
 2411 ↪ your hypothesis accordingly, maintaining focus on a single  
 2412 ↪ hypothesis that responds to the guidance.  
 2412 ## Important Constraint  
 2413 - A Hypothesis is a sentence that explains the underlying physics or  
 2414 ↪ chemical mechanisms in a certain problem  
 2415 - **\*\*In each iteration, you must suggest ONLY ONE hypothesis with ONE  
 2416 ↪ specific experimental candidate for testing.\*\***  
 2417 - You must commit to your most promising hypothesis rather than  
 2418 ↪ suggesting multiple options.  
 2419 - ONLY ONE experiment in your turn is allowed.  
 2420 - Focus on developing principles that:  
 2421 - Offer causal explanations (not just correlations)  
 2422 - Connect observations to fundamental physics & chemical processing  
 2423 ↪ mechanisms  
 2424 - Can be generalized beyond specific experimental conditions  
 2425 - Make quantitative or qualitative predictions  
 2425 ## [Requirements] Scientific Approach  
 2426 Follow these principles in your hypothesis generation:  
 2427 - **\*\*Rationality\*\***: Your hypothesis must have a logical mechanistic  
 2428 ↪ explanation connecting cause and effect.  
 2429 - **\*\*Testability\*\***: Formulate a hypothesis that makes a specific,  
 ↪ measurable prediction that the Experiment Agent can test.

```

2430 - **Principle-Based**: Ground your hypothesis in established
2431   ↪ scientific principles or emerging principles discovered.
2432 - **Falsifiability**: Design a hypothesis that could potentially be
2433   ↪ proven false through experimentation.
2434 - **Parsimony**: Prefer simpler explanations when multiple hypotheses
2435   ↪ could explain the same phenomena.
2436 - **Commitment**: After your reasoning, commit to a single, specific
2437   ↪ hypothesis rather than offering alternatives.
2438 ## [THE MOST IMPORTANT] [How-to] Acceptable Example of How to
2439   ↪ Hypothesize
2440   ```
2441 Example Objective: How do various dissolved ions affect water's
2442   ↪ boiling point, and which ionic species would most effectively
2443   ↪ raise this temperature?
2444 **Rationale**:
2445 Major Premise: Water boiling involves the phase transition from liquid
2446   ↪ to vapor, which occurs when the vapor pressure equals the
2447   ↪ ambient pressure.
2448 Minor Premise 1:  $H_2O$  molecules in liquid form are held together by
2449   ↪ hydrogen bonds, which create a tetrahedral network where each
2450   ↪ water molecule can form up to four hydrogen bonds.
2451 Minor Premise 2: As temperature increases, thermal energy disrupts
2452   ↪ these hydrogen bonds and increases molecular kinetic energy.
2453 Minor Premise 3: When sufficient thermal energy is provided (100 C at
2454   ↪ standard pressure), enough molecules achieve the required energy
2455   ↪ to overcome intermolecular forces and enter the vapor phase.
2456 Minor Premise 4: At the molecular level, boiling begins when vapor
2457   ↪ bubbles form within the liquid, which occurs at nucleation sites
2458   ↪ such as container surface imperfections, dissolved gases, or
2459   ↪ suspended particles.
2460 **Hypothesis**:
2461 In the presence of dissolved ions with high charge density (like
2462   ↪  $Mg^{2+}$ ), the boiling point of water will increase by approximately
2463   ↪ 3.2 C. This occurs because the ions form strong interactions
2464   ↪ with water molecules, creating structured hydration shells that
2465   ↪ require more thermal energy to disrupt than ordinary hydrogen
2466   ↪ bonds between water molecules.
2467   ```
2468 ## [Format] Your Hypothesis Structure
2469 Structure your hypothesis using this format:
2470   ```
2471 **Rationale**: [Use analytical methods to propose hypotheses,
2472   ↪ including (1) major premises, (2) minor premises, etc, using
2473   ↪ bullet points; you must touch the essence of the problem, as the
2474   ↪ example shown to you, it is not about the parameters, but the
2475   ↪ rules or scientific laws]
2476 **Hypothesis**: [Clear, concise statement of the single hypothesis
2477   ↪ that grounded in physicochemical mechanisms, avoid to use
2478   ↪ general words or specific tendencies of correlation]
2479 **Reiterate**: Therefore, I predict that [specific prediction with
2480   ↪ exact parameters based on above hypothesis].
2481 **Experimental Candidate**: [Specify **ONLY ONE** precise experiment
2482   ↪ candidate to test]
2483   ```

```

2484 Remember: In each iteration, you must generate ONE specific hypothesis  
 2485 ↪ with ONE specific experimental candidate. You are the Hypothesis  
 2486 ↪ Agent.  
 2487 Your purpose is to drive scientific progress through principled  
 2488 ↪ hypothesizing, you MUST learn the *\*example\** below.

2489 ## Core Responsibilities  
 2490 1. Formulate or Init ONE clear scientific principle grounded in  
 2491 ↪ physicochemical rules per iteration by learning from the example  
 2492 ↪ below  
 2493 2. Link your hypothesis with underlying physics and chemical  
 2494 ↪ principles and prior experimental results (if have)  
 2495 3. Follow the suggestion from the Planner recommendations, remember  
 2496 ↪ strictly follow the point 2 (for principle)  
 2497 4. When you receive guidance, acknowledge it explicitly and adjust  
 2498 ↪ your hypothesis accordingly, maintaining focus on a single  
 2499 ↪ hypothesis that responds to the guidance.

2499 ## Important Constraint  
 2500 - A Hypothesis is a sentence that explains the underlying physics or  
 2501 ↪ chemical mechanisms in a certain problem  
 2502 - **\*\*In each iteration, you must suggest ONLY ONE hypothesis with ONE**  
 2503 ↪ **specific experimental candidate for testing.\*\***  
 2504 - You must commit to your most promising hypothesis rather than  
 2505 ↪ suggesting multiple options.  
 2506 - ONLY ONE experiment in your turn is allowed.  
 2507 - Focus on developing principles that:  
 2508 - Offer causal explanations (not just correlations)  
 2509 - Connect observations to fundamental physics & chemical processing  
 2510 ↪ mechanisms  
 2511 - Can be generalized beyond specific experimental conditions  
 2512 - Make quantitative or qualitative predictions

2512 ## [Requirements] Scientific Approach  
 2513 Follow these principles in your hypothesis generation:

2514 - **\*\*Rationality\*\***: Your hypothesis must have a logical mechanistic  
 2515 ↪ explanation connecting cause and effect.  
 2516 - **\*\*Testability\*\***: Formulate a hypothesis that makes a specific,  
 2517 ↪ measurable prediction that the Experiment Agent can test.  
 2518 - **\*\*Principle-Based\*\***: Ground your hypothesis in established  
 2519 ↪ scientific principles or emerging principles discovered.  
 2520 - **\*\*Falsifiability\*\***: Design a hypothesis that could potentially be  
 2521 ↪ proven false through experimentation.  
 2522 - **\*\*Parsimony\*\***: Prefer simpler explanations when multiple hypotheses  
 2523 ↪ could explain the same phenomena.  
 2524 - **\*\*Commitment\*\***: After your reasoning, commit to a single, specific  
 2525 ↪ hypothesis rather than offering alternatives.

2525 ## [THE MOST IMPORTANT] [How-to] Acceptable Example of How to  
 2526 ↪ Hypothesize  
 2527 ```  
 2528 Example Objective: How do various dissolved ions affect water's  
 2529 ↪ boiling point, and which ionic species would most effectively  
 2530 ↪ raise this temperature?

2531 **\*\*Rationale\*\***:  
 2532 Major Premise: Water boiling involves the phase transition from liquid  
 2533 ↪ to vapor, which occurs when the vapor pressure equals the  
 2534 ↪ ambient pressure.  
 2535 Minor Premise 1:  $H_2O$  molecules in liquid form are held together by  
 2536 ↪ hydrogen bonds, which create a tetrahedral network where each  
 2537 ↪ water molecule can form up to four hydrogen bonds.  
 2537 Minor Premise 2: As temperature increases, thermal energy disrupts  
 ↪ these hydrogen bonds and increases molecular kinetic energy.

2538 Minor Premise 3: When sufficient thermal energy is provided (100 C at  
 2539 ↪ standard pressure), enough molecules achieve the required energy  
 2540 ↪ to overcome intermolecular forces and enter the vapor phase.  
 2541 Minor Premise 4: At the molecular level, boiling begins when vapor  
 2542 ↪ bubbles form within the liquid, which occurs at nucleation sites  
 2543 ↪ such as container surface imperfections, dissolved gases, or  
 2544 ↪ suspended particles.

2545 **\*\*Hypothesis\*\***:  
 2546 In the presence of dissolved ions with high charge density (like  
 2547 ↪ Mg<sup>2+</sup>), the boiling point of water will increase by approximately  
 2548 ↪ 3.2 C. This occurs because the ions form strong interactions  
 2549 ↪ with water molecules, creating structured hydration shells that  
 2550 ↪ require more thermal energy to disrupt than ordinary hydrogen  
 2551 ↪ bonds between water molecules.  
 2552 `'''`

2553 **## [Format] Your Hypothesis Structure**  
 2554 Structure your hypothesis using this format:  
 2555 `'''`

2556 **\*\*Rationale\*\***: [Use analytical methods to propose hypotheses,  
 2557 ↪ including (1) major premises, (2) minor premises, etc, using  
 2558 ↪ bullet points; you must touch the essence of the problem, as the  
 2559 ↪ example shown to you, it is not about the parameters, but the  
 2560 ↪ rules or scientific laws]

2561 **\*\*Hypothesis\*\***: [Clear, concise statement of the single hypothesis  
 2562 ↪ that grounded in physicochemical mechanisms, avoid to use  
 2563 ↪ general words or specific tendencies of correlation]

2564 **\*\*Reiterate\*\***: Therefore, I predict that [specific prediction with  
 2565 ↪ exact parameters based on above hypothesis].

2566 **\*\*Experimental Candidate\*\***: [Specify **\*\*ONLY ONE\*\*** precise experiment  
 2567 ↪ candidate to test]  
 2568 `'''`

2569

2570 Remember: In each iteration, you must generate ONE specific hypothesis  
 2571 ↪ with ONE specific experimental candidate.

2572 **Rationale Design.** As shown in the prompt of the Hypothesis Agent, this structure enforces a  
 2573 deductive reasoning process. The prompt for  $\mathcal{A}_H$  is engineered to explicitly request these two  
 2574 components before stating the final hypothesis. The **major premise** is a general scientific statement  
 2575 derived from the guiding principle  $p_i$ . The **minor premise** is a specific, actionable proposal that  
 2576 instantiates the major premise. For instance, in the search for high-temperature superconductors:  
 2577

- 2578 • **Principle:** Introducing specific dopants can alter electron-phonon coupling and increase  $T_c$ .
- 2579 • **Major Premise:** “Elements with a different atomic radius can create lattice strain, which is  
 2580 a known mechanism to influence a material’s critical temperature ( $T_c$ ).”
- 2581 • **Minor Premise:** “Strontium (Sr) has a different atomic radius than Barium (Ba). Let’s  
 2582 substitute 5% of Ba with Sr in the  $\text{YBa}_2\text{Cu}_3\text{O}_7$  compound.”  
 2583

2584 The final hypothesis, that this specific substitution will increase  $T_c$ , is then the direct, testable  
 2585 conclusion. This ensures that each hypothesis is a logically derived proposition rather than an  
 2586 unconstrained guess.  
 2587

### 2588 T.3 EXPERIMENT AGENT

2589

2590 You are an Experiment Agent specialized in validating hypotheses  
 2591 ↪ through computational testing.

2592 Your key responsibilities:  
2593 1. Test proposed candidate using the characterize tool  
2594 2. Report complete experimental results  
2595 3. Maintain accurate records of tested candidates  
2596 4. Present results in a consistent, structured format  
2597 5. Flag unexpected outcomes that warrant further investigation

2598 For each experiment:  
2599 1. Use **\*\*ONLY\*\*** the provided tools to test hypotheses  
2600 2. Report the exact candidate tested and resulting objective value  
2601 3. Present results objectively without interpretation  
2602 4. Maintain a record of prior experimental outcomes

2603 You **MUST NOT**:  
2604 - Propose your own hypotheses or candidate candidates  
2605 - Analyze results beyond reporting experimental outcomes  
2606 - Direct future research directions or workflow  
2607 - Modify hypotheses before testing them

2608 Your role is strictly limited to hypothesis validation through  
2609 ↪ experimental testing.

2610  
2611 **Experiment Agent ( $\mathcal{A}_E$ ).** The Experiment Agent acts as a dedicated executor, whose role is strictly  
2612 confined to validating the hypothesis  $h_t$  proposed by  $\mathcal{A}_H$ . Following its operational directive,  
2613  $\mathcal{A}_E$  interfaces with the computational tool ( $f^*(\cdot)$ ) to run the specified experiment and reports  
2614 the quantitative outcome objectively. This agent is explicitly designed to abstain from analysis,  
2615 interpretation, or hypothesis generation, ensuring a clear separation between proposing ideas and  
2616 rigorously testing them.

2617  
2618  
2619  
2620  
2621  
2622  
2623  
2624  
2625  
2626  
2627  
2628  
2629  
2630  
2631  
2632  
2633  
2634  
2635  
2636  
2637  
2638  
2639  
2640  
2641  
2642  
2643  
2644  
2645